THE IMPLEMENTATION AND EVALUATION OF A BLACK CARBON AEROSOL SAMPLER USED ON AN UNMANNED AIRCRAFT DURING THE PRESCRIBED FIRE EXPERIMENT RXCADRE
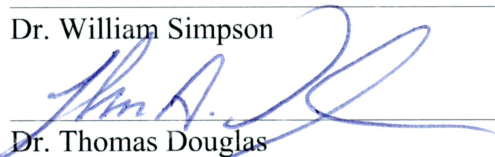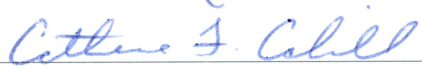
By

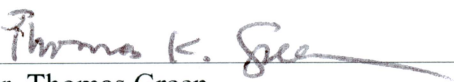Tara L. Craft

RECOMMENDED:

Dr. William Simpson

Dr. Thomas Douglas

Dr. Catherine Cahill
Advisory Committee Chair
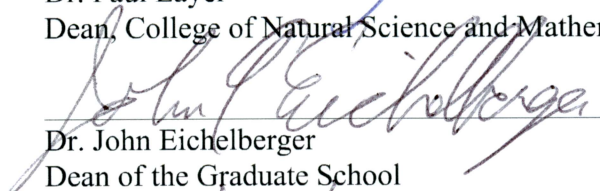
Dr. Thomas Green
Chair, Department of Chemistry and Biochemistry
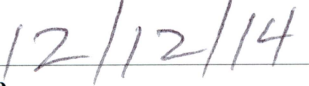
APPROVED:

Dr. Paul Layer
Dean, College of Natural Science and Mathematics

Dr. John Eichelberger
Dean of the Graduate School

12/12/14
Date

THE IMPLEMENTATION AND EVALUATION OF A BLACK CARBON AEROSOL

SAMPLER USED ON AN UNMANNED AIRCRAFT DURING THE PRESCRIBED FIRE

EXPERIMENT RXCADRE

A

THESIS

Presented to the Faculty

of the University of Alaska Fairbanks

in Partial Fulfillment of the Requirements

for the Degree of

MASTER OF SCIENCE

By

Tara L. Craft, B.S.

Fairbanks, Alaska

December 2014

Abstract

Black carbon (BC) aerosols impact the earth's climate by absorbing solar radiation in the atmosphere and depositing on ice surfaces and lowering the albedo of those surfaces. Black carbon aerosols have been widely studied; however, using small unmanned aircraft systems (UAS) for the airborne study of the vertical and horizontal concentrations of BC is an emerging field. Using UAS to study BC poses some challenges due to size and weight restrictions of the aircraft, as well as issues that arise when adapting ground based instrumentation for use on different aircraft. University of Alaska Fairbanks researchers successfully integrated and flew a microAeth AE-51 on a Boeing ScanEagle to measure the concentration of BC and other absorbing and scattering particles in the smoke plume from a prescribed fire experiment, RxCADRE, conducted at Eglin AFB, FL, during October and November 2012. The ScanEagle-mounted microAeth successfully collected black carbon aerosols in the smoke plume. The optical particle sizing and mass loadings from an optical particle counter disagreed with the results from the microAeth, which measures absorbing aerosols. The microAeth was tested in the laboratory-using two optical particle sizers to verify the sizes and concentrations of laboratory-generated aerosols entering the instrument and determine the capabilities and limits of the instrument. The optical particle counters were used in other applications as well showing the versatility of the instruments in extreme conditions.

Table of Contents

List of Figures

Chapter 1 – Introduction

Particles suspended in the atmosphere, known as atmospheric aerosols, have impacts that range from local to global scales. Local impacts include urban air pollution[1,2] that can result in adverse human health effects.[3] Global impacts include changes in the earth's radiative balance that can influence global climate. Therefore, scientists must determine the concentrations and compositions of aerosols throughout the atmosphere to quantify the magnitude of these effects.

1.1 Aerosols

The term aerosol refers to an assembly of liquid or solid particles suspended in a gaseous medium long enough to be observed or measured.[4] Some examples of aerosols are airborne dust and smoke. Aerosols are found everywhere in the environment and can have significant impacts on the atmosphere as well as severe physiological effects. Aerosols have a wide range of shapes and sizes that make it difficult to define a typical aerosol, but scientists use the concept of an aerodynamic diameter to help generalize how aerosols move in an airflow. The aerodynamic diameter of a particle is the diameter of a perfectly spherical reference aerosol of 1 g cm^{-1} density that demonstrates the same behavior in an airflow as the particle of interest.[4] Particulate matter (PM) 2.5 and particulate matter 10, which are particulate matter with an aerodynamic diameter of two and a half microns (μm) or less, and ten μm or less, respectively, are the most talked about aerosol size fractions when discussing health effects and visibility degradation. For the remainder of this thesis, PM 2.5 and PM 10 will be depicted as $PM_{2.5}$ and PM_{10}, respectively.

Particle size is the most important descriptor for predicting aerosol impacts[2] because it determines the behavior of the particle suspended in a gas[4], how the particle can be measured,

and what potential impacts the aerosol may have.[4] For example, the smaller the particle, the greater the chances are that the aerosols will interact with light or enter the deep lung and cause physiological effects. Also, many aerosols are so small that they do not settle out of the atmosphere quickly and can impact places far downwind of their sources. Aerosols can range in size from a few nanometers (10^{-9} meters) to the thickness of a human hair, or even larger. The United States Environmental Protection Agency (U.S. EPA) created Figure 1.1, which provides a size comparison to show the sizes of aerosols with respect to items the public can visualize. Figure 1.2[5] shows an idealized trimodal distribution of aerosol size as a function of formation mechanism and the mechanisms by which they become larger aerosols. The dashed line represents where an aerosol reaches the $PM_{2.5}$ size fraction. The particles in the size range of 0.001 μm to 0.1 μm are known as Aitken particles. These are the smallest of the size fractions for particles. Aitken particles are formed when hot vapors that are lofted into the air condense into particles as they cool. Water can condense onto the particles causing them to grow larger. The particles can then strike each other and coagulate, becoming even larger particles and entering the accumulation mode. Many of the aerosols in the accumulation mode are secondary aerosols. Secondary aerosols are a result of gas-to-particle conversions. Gaseous chemical reactions form low volatility vapors that then condense and form secondary particles.[6,7] The size range for a particle in the accumulation mode is approximately 0.1 μm to 2.5 μm. Once the aerosols become bigger than approximately 2.5 μm in aerodynamic diameter, they have an appreciable settling velocity and fall out of the atmosphere. However, particles in the accumulation mode do not grow quickly by coagulation or rapidly settle out of the atmosphere, so they get 'stuck' in this mode until water can condense on them and make the particles big enough to wash out of the atmosphere.

Stokes found that the resisting force exerted by air on a moving particle is equivalent to the force exerted by moving air on a stationary particle.[8] Stokes' Law (Equation 1.1) is used to predict the settling velocity of a sphere moving through a medium.

$$v_s = \frac{2}{9}\frac{(\rho_p - \rho_f)}{\mu} g\, R^2$$

(1.1)

In Equation 1.1, v_s is the settling velocity, μ is the viscosity of the medium, ρ_p is the density of the particle, ρ_f is the density of the fluid (air), R is the radius, and g is gravity.[8] Typical settling velocities for particles of aerodynamic diameter 0.1, 1.0, and 10 microns are approximately $9x10^{-7}$, $4x10^{-5}$, and $3x10^{-3}$, respectively[8], therefore, the larger particles fall out far more quickly than the smaller particles.

The majority of smaller aerosols are the result of combustion, including high temperature industrial combustion and wildfires. Coarse particles are defined as any aerosols that are larger than 2.5 µm. Most coarse particles are generated naturally and can include sea salt aerosols, volcanic ash, dust, and other aerosols that occur naturally in the environment.   High concentrations of larger aerosols are found close to their source, but their concentrations decrease rapidly with the distance away from their origin due to their high settling velocities.
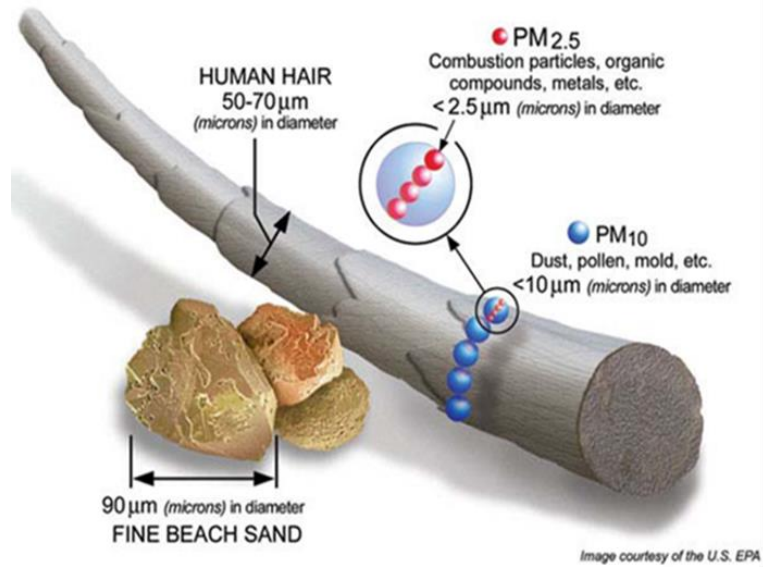
Figure 1.1. Image provided by the U.S. EPA of a size comparison for aerosol particle size.
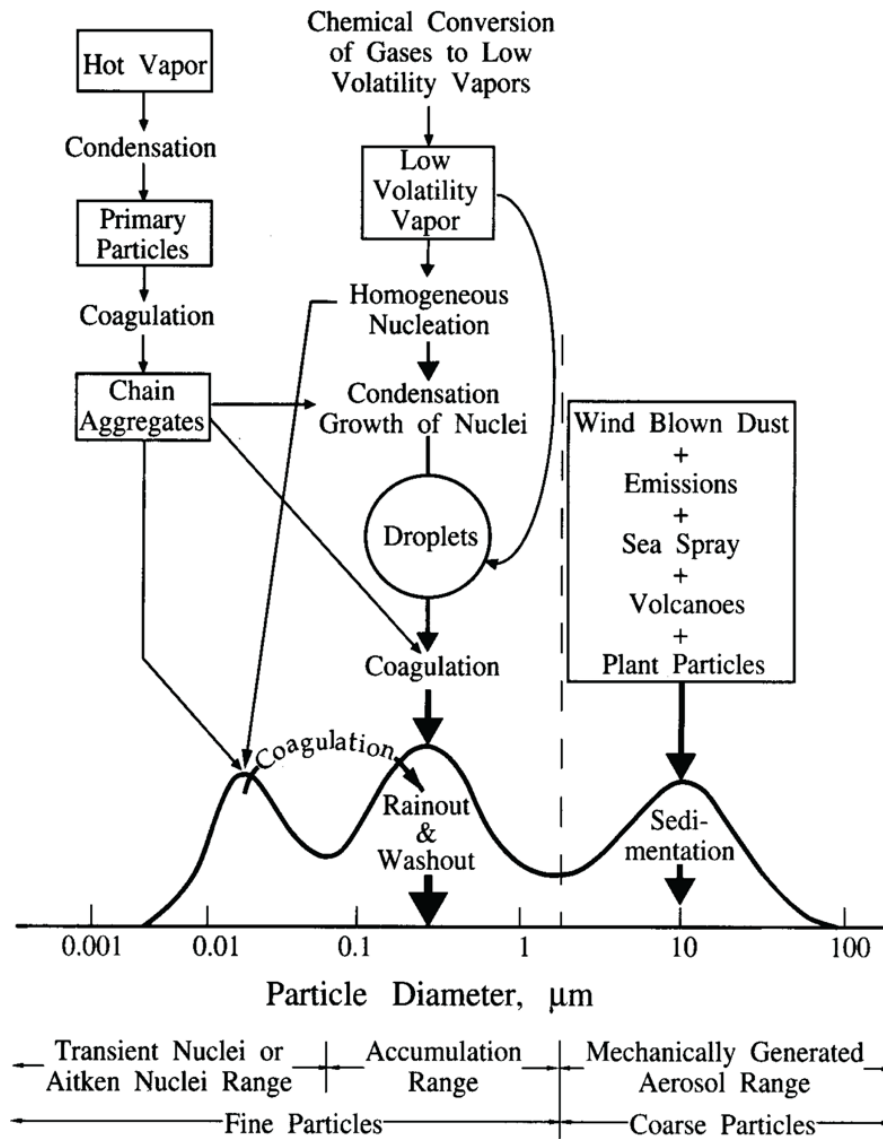
Figure 1.2. Idealized schematic of the distribution of particle surface area of an atmospheric aerosol.[5] Principal modes, sources, and particle formation and removal mechanisms are indicated.

1.2 Effects of Aerosols

It is important to be familiar with the effects associated with aerosols because aerosols can have observable impacts from local to global scales. These impacts include adverse human health effects, threats to aviation, ecosystem impacts, and climate changes.

Particles with a diameter of one micron or less act as vehicles transporting toxic chemicals into the human respiratory system.[9] Increased reports of asthma and bronchitis have been related to increasing particle concentrations.[10] In extreme cases, the high particle concentrations can lead to decreased lung functions, stroke, and even premature death in humans.[10-12] With every increase of ten micrograms per cubic meter ($\mu g\ m^{-3}$) in fine particulate matter, there is approximately a six percent increased risk of fatal heart attacks, and an eight percent increase in risk of lung cancer fatalities.[11]

Aviation companies are highly concerned about the aerosols emitted into the atmosphere. Volcanic eruptions loft large quantities of volcanic ash into the atmosphere that pose a threat to aircraft. If an aircraft flies through a volcanic plume, the ash could get sucked into the engine, heated until it essentially becomes molten rock, block the cooling vents for the engine, and cause engine failure[13], which could potentially bring down the aircraft. Volcanic ash also degrades the aircraft, such as stripping off the paint and etching the windows. In 1989, a Boeing 747 aircraft flew through a volcanic ash cloud from the Redoubt volcano eruption approximately one hundred miles south west of Anchorage, Alaska. There was significant damage to the aircraft's engines, avionics, and airframe.[13] The damages were estimated to be $80 million dollars.[13] It is important for aviation companies to understand the composition and size of aerosols being emitted by a volcanic eruption to develop methods to mitigate the effects of aerosols in their engines when a plane strikes a volcanic plume.

6

Aerosols can also impact ecosystems. Nutrient (and pollutant) transport plays a vital role in ecosystem balance and stability. Aerosols from different sources can be deposited to distant ecosystems and change the productiveness of those ecosystems. Wind can pick up particles from a land surface, particularly when the soil is dry and without plant cover, and carry the particles great distances away from the source region before depositing the particles back to the Earth's surface. For example, dust from the African Sahara Desert is frequently mixed through a deep layer of the atmosphere and transported westward across the Atlantic Ocean by the Trade Winds until the material is deposited throughout the Caribbean and the United States.[14] Soils from the Gobi and Taklimakan Deserts in Asia can transport to Hawaii, Alaska, and the western coast of the United States where they are deposited to ecosystems.[15,16] The pollutants and nutrients associated with the soil can enhance productivity or damage ecosystems.[17]

The role of aerosols in climate continues to be a major area of research. Wildfire aerosols, in particular, black carbon (BC) aerosols, are important to study because of how they influence the climate by absorbing and scattering long and short-wave radiation, which can lead to heating or cooling of the Earth's surface.

1.3 Black Carbon Aerosols

Black carbon (BC) is a primary aerosol, emitted directly at the source from incomplete combustion processes. Black carbon is also commonly referred to as soot[18] and it is a major contributor to radiative forcing.[19] Sources of BC include fossil fuel combustion and biomass burning.[18,20] Much of the atmospheric BC is of anthropogenic origin[21], but wildfires account for at least 40% of global black carbon production.[19] More than ninety percent of BC resides in the $PM_{2.5}$ size fraction.[22] Black carbon has a short atmospheric lifetime of about one week[23,24]

because BC can be removed from the atmosphere by both wet and dry deposition. When BC gets removed from the atmosphere by rain and snowfall[25], and is deposited onto surfaces, such as snow and ice[19], the albedo of the Earth's surface decreases.[19,22,26] This change in albedo decreases how much solar radiation is reflected from these light surfaces and causes an increased melting of the snow[19] and ice around the deposited particles as the dark BC particles absorb the solar radiation, heat up, and melt the snow and ice around them. General circulation climate models (GCMs) suggest that the reduction of sea ice and snow albedo by BC is three times as effective as CO_2 forcing for global average surface warming.[26]

1.4 Unmanned Aircraft System (UAS) Aerosol Measurements

The horizontal and vertical distributions of aerosols in the atmosphere are vital to understanding the effects of aerosols on the radiative forcing in the atmosphere and how the aerosols will transport. There are many publications on sampling the horizontal and vertical distribution of aerosols using manned aircraft; however there are very few studies that measure the spatial distribution of aerosols using unmanned aircraft. Unmanned Aircraft System (UAS) based aerosol sampling allows scientists to view aerosols in the atmosphere in three dimensions in a variety of different environments, including hazardous ones, without the risk and expense of flying a manned aircraft.

Unmanned aircraft have been used in a wide variety of research campaigns; however, most of the current research that uses UASs utilizes the surveillance capabilities of the aircraft.[27] Only recently have several studies been done that use UASs for collecting real-time gas and aerosol measurements.

A Thunder Tiger Raptor 90 helicopter[28] was used in a campaign to record the very first measurements of volcanic gases with an unmanned aircraft. The team of researchers were from Europe and they were specifically looking at measurements of volcanic carbon dioxide fluxes from La Fossa crater, Vulcano, Italy.[28] The payloads used in this research were: an ultraviolet spectrometer for measuring sulfur dioxide fluxes, an infrared spectrometer for measuring carbon dioxide concentrations, and an electrochemical sensor for sulfur dioxide concentrations.[28] The data collected helped the researchers confirm the excellent potential of a rotor UAV for use in volcanology.[28]

The Maldives Autonomous UAV (unmanned aerial vehicle) Campaign (MAC)[29-31] showed how versatile using a UAS could be. The MAC demonstrated the ability to observe aerosol and cloud microphysical properties and solar radiation fluxes simultaneously[30] by using three UAVs flown in a stacked orientation, one sampling at cloud level[30], one sampling below the clouds[29], and one sampling above the clouds.[29,30] The aircraft platforms used for the study were Advanced Ceramics Research (ACR) Mantas.[31] The researchers flew an absorption photometer adapted from a Magee Scientific AE-31 seven wavelength aethalometer.[31] This modified instrument measured aerosol optical absorption at 370, 520, and 880 nm.[29] The stacked UAVs provided simultaneous measurements of aerosols, black carbon, cloud microphysics and solar radiation fluxes around clouds.[29]

1.4.1 Advantages to UASs versus Manned Aircraft

There are many advantages to using a UAS instead of a manned aircraft. A UAS can fly in hazardous areas and collect real-time air samples without putting humans at risk. They are less expensive[27] than manned aircraft and are also less expensive to maintain in the long-term.

The UAS is more versatile to maneuver and has longer dwell times, meaning it can stay in the air longer, than a manned aircraft. Aircraft pilots can only stay in the air for a certain amount of time before they need to take a mandatory rest period. Unmanned aircraft systems can stay airborne as long as their fuel will allow.

1.4.2 Disadvantages to UASs versus Manned Aircraft

While there are many advantages to using a UAS, there are some disadvantages as well. The FAA (Federal Aviation Administration) has tighter regulations for using a UAS versus a manned aircraft. In some cases, the FAA needs to be contacted years in advance of the UAS flight. A two-way data link is used in UASs to send the data collected from the sensors to the ground station and to provide the control of the unmanned aircraft systems.[27] If the data link becomes compromised, or stops relaying information, the information collected could be lost as could control of the UAS. Situational awareness can be a problem for unmanned aircraft because the UAS operator never has a full view of the airspace[27,32], like a pilot would. Typically the UAS platform is smaller than a manned aircraft so the payload weight and size capabilities are restricted. Filter saturation for onboard sensors is also an issue, especially if the sensor needs to have filter strips changed out periodically. If the filter changing is autonomous then the UAS can stay airborne until the end of sampling. If the filter needs to be changed manually; either the aircraft needs to be grounded during sampling, or the instrument does not collect samples for the entire duration of the flight.

1.5 Thesis Goals

A Boeing ScanEagle[33] was the UAS used for the experiments in this thesis. The UAS was important for the aerosol sampling because it provided the opportunity to study the aerosols

in three dimensions. The UAS also provided real-time data of the aerosols inside the smoke plume. This thesis peers into the first ever integration of a microAethalometer on a Boeing ScanEagle.

There is currently a wide range of sensors that allow for the measurement of aerosols, in particular; BC. There is not, however, a wide range of sensors that allow for the airborne measurement of BC aerosols using small UAS. Currently, the aerosol measuring capabilities on small UAS are basically non-existent due to payload weight and size restrictions. The successful adaptation and integration of ground-based aerosol sensors on UASs will allow for more understanding of the spatial and temporal distribution of aerosol mass concentration, composition, and size. This thesis will discuss the successful integration of a micro-aethalometer, an instrument that measures BC, onto a University of Alaska Fairbanks (UAF) UAS during a 2012 field campaign, Prescribed Fire Combustion-Atmospheric Dynamic Research Experiments (RxCADRE), at Eglin Air Force Base, Florida. This thesis will also characterize the microAethalometer so that it may be used on other unmanned aircraft. Other projects that tested and used the aerosol equipment used at RxCADRE and aethalometer sampling that took place during the summer 2013 fire season in Fairbanks, Alaska, will also be discussed.

Chapter 2 – Experimental Methods

2.1 RxCADRE Campaign

The Prescribed Fire Combustion-Atmospheric Dynamic Research Experiments (RxCADRE) campaign in November 2012 was funded by the interagency Joint Fire Science Program to conduct a third campaign in non-forested fuels. The first two campaigns were successfully conducted in 2008 and 2011. The 2012 RxCADRE team was interagency and had representatives from the Department of Defense (DoD), NASA, academia, and other agencies. The team was also multidisciplinary (ecology, fire physics, remote sensing, etc.).

The primary objectives for RxCADRE 2012 included producing data sets for smoke chemistry, transport, and fire behavior models. Secondary objectives included ecological measurements and coordination with satellite observation. During a large plot burn there were six aircraft, from multiple institutions, orbiting simultaneously over the plot and providing an excellent demonstration of airspace deconfliction. There were two manned aircraft (Cessna 206, and Piper Navajo fitted with a Wildfire Airborne Sensor Program [WASP] package), and four unmanned aircraft systems (2-G2Rs, an Aeryon Scout, and a Boeing ScanEagle), collecting different sets of data during the prescribed burn.

2.1.1 The Sampling Site

The RxCADRE campaign took place at Eglin Air Force Base in Florida (Figure 2.1). The base is located on Florida's panhandle approximately three miles southwest of Valparaiso, FL. The climate is typically dry, making Eglin AFB an ideal location for a prescribed burn.

There were three small plot burns (Figures 2.2 and 2.3) of approximately 5 to 10 acres each, as well as one large plot burn (Figures 2.2 and 2.4) of approximately 1600 acres. The small and large plots contained uniformly distributed grass fuels.
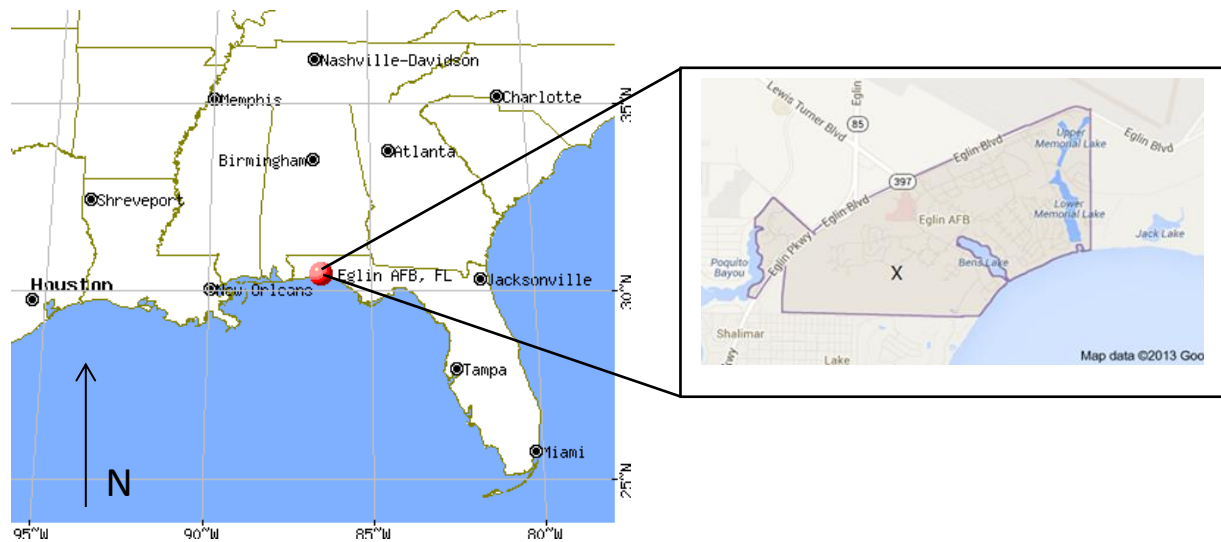
Figure 2.1. The location of Eglin Air Force Base (AFB) is represented by a red circle. Eglin AFB is located approximately three miles southwest of Valparaiso, Florida. Image provided by City-Data.com. The expanded image on the right shows the Eglin Air Force Base boundaries. The "x" on the map shows the location of the prescribed burns during the RxCADRE campaign. Image provided by Google Maps.
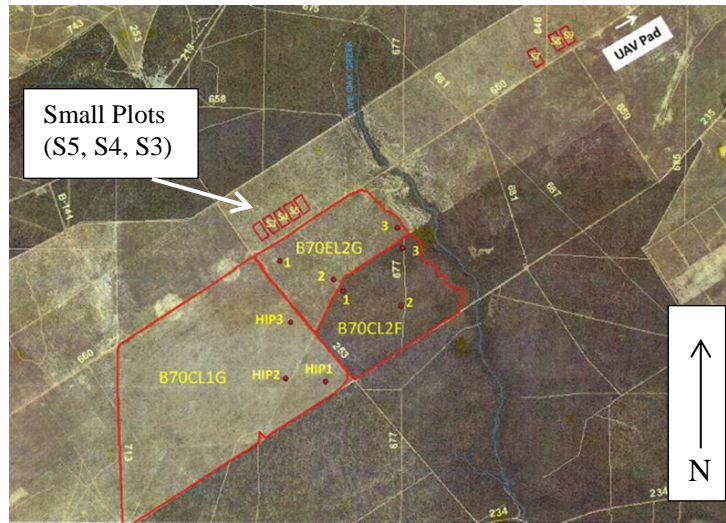
Figure 2.2. Location of small plots (S5, S4, S3) in relation to the large plot (B70CL1G). The small and large plots are separated by a dirt road. Image provided by RxCADRE personnel.

Figure 2.3. The layout of the small plot burns. Each plot was roughly 5 to 10 acres. The first fire was on S5, the second on S4, and the last one on S3. The white line under the plots was a dirt road that may have contributed some non-smoke aerosol to our aerosol samples. Image adapted from Google Earth.
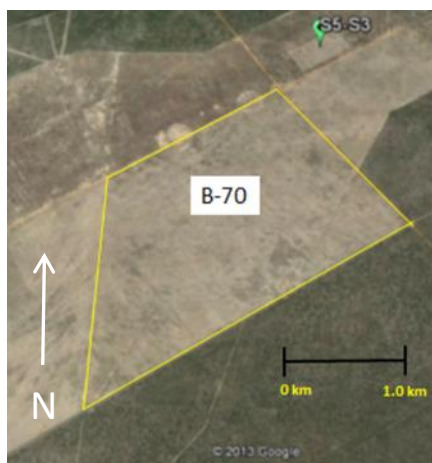
Figure 2.4. Image showing the layout of the large plot burn, which was roughly 16 acres. The small plot burns are shown by the green marker labeled S5-S3. Image adapted from Google Earth.

2.2 Instrumentation

2.2.1 microAethalometers

The microAethalometer[34] is a recently-developed miniature instrument that makes a real-time measurement of BC on a very short time base in a self-contained, battery-powered package that is lightweight and pocket sized.[35] The microAethalometer, from Aethlabs in San Francisco, California, is an instrument that measures the concentration of optically absorbing and scattering particles based on their aerodynamic diameter. The aethalometer estimates the BC mass concentrations from the rate of change of light transmission through an aerosol deposited on a three millimeter diameter portion of T60 Teflon-coated borosilicate glass fiber filter (Figure 2.5).[24]

The microAeth obtains the concentration of aerosols by drawing an air sample through the filter. Optical transmission through the three millimeter portion is measured by a stabilized light source and photo diode detector. The gradual increase in particles collected leads to the gradual increase in light absorption from one sample to the next. The air flow rate through the filter is measured by a mass flow sensor which is also used to stabilize the pump. The electronics and microprocessor measure and store the data from each sample to determine the increment during each time base (microAeth AE-51 operating manual). Using the known absorbance (per unit) of BC, the increment determined by the electronics is converted to a mass concentration of BC expressed in nanograms per cubic meter (ng m^{-3}).

(2.1) $$I = I_0 e^{-b_{abs} \cdot x}$$

Equation 2.1 shows Beer's Law, where I_0 is the intensity of the incoming light and I represents the remaining light intensity after passing through a medium with the thickness x.[36] Beer's Law illustrates the relationship between the absorbance and concentration of the particles collected on the filter strip. Aethalometers measure the attenuation which is the natural log (ln) of the ratio I/I_0.

Two microAeths were used at RxCADRE: the first was a single wavelength, AE-51, (Figure 2.6a) that measures optically absorbing particles at 880 nm, which is interpreted as the concentration of black carbon; and the second microAeth, AE-52, (Figure 2.6b) is a multi-wavelength sensor that measures the light attenuation due to both absorbing and scattering particles at 880 nm and 370 nm, respectively. The ultraviolet particulate matter (UVPM) channel is interpreted as light attenuation by any particle not considered black carbon, and provides an estimate of the total particulate concentration for each sampling event. Certain organic aerosol components of wood burning particles have enhanced optical absorption at 370 nm relative to 880 nm.[37-39] The difference between the 370 nm signal and the 880 nm signal has been suggested to serve as an indicator of wood burning particles.[24]

Both microAeths have a preferred measurement range of 0 to 1 mg BC m^{-3}, with measurement precision ±0.1 µg BC m^{-3}. The microAeths weigh approximately 0.62 lbs. (280 g) and have the following dimensions: 4.6 in. (117 mm) length x 2.6 in. (66 mm) width x 1.5 in. (38 mm) depth. Both instruments were designed for ground-based operation. One of the main goals of the UAF aerosol team participating in the campaign was to adapt one of the microAeths, the AE-51, for airborne use on the Boeing ScanEagle unmanned aircraft.

Additionally, from March 2013 to May 2013, both microAethalometers were used on a solo flight from Fairbanks, AK to the geographic North Pole. The aircraft used for the flight was the "Polar Pumpkin" (Figure 2.7) which was a Cessna 185, piloted by Art Mortvedt. The scientific goal for the flight was to sample airborne black carbon throughout the Canadian Archipelago and across the Arctic Ocean to the North Pole. The data collected during sampling would allow for the observation of the effectiveness of the microAeths in high altitude (the minimum "safe" altitude was 6,000 feet), heavy wind, and extreme temperature conditions. The AE-51 microAeth was set to record data every one second with a flow rate of 150 mlpm. The AE-52 microAeth recorded data every sixty seconds with the flow rate set to 100 mlpm. The flow rates were set higher to accommodate the speed of the air entering the inlet chamber.

The multi-wavelength aethalometer, AE-52, was also used to record aerosols emitted from the Nenana, AK fire in June 2013. The fire burned more than 80 acres of white spruce and was located approximately 30 miles south of Fairbanks, at mile 324 on the Parks Highway. The AE-52 was recording data every ten seconds with the flow rate set to 50 mlpm. The inlet tube of the microAeth stuck out of a port hole in a window in Dr. Catherine Cahill's laboratory at the Syun Ichi Akasofu Building on the campus of the University of Alaska Fairbanks in Fairbanks, AK. The port hole faced south and was thirty feet (nine meters) off of the ground.
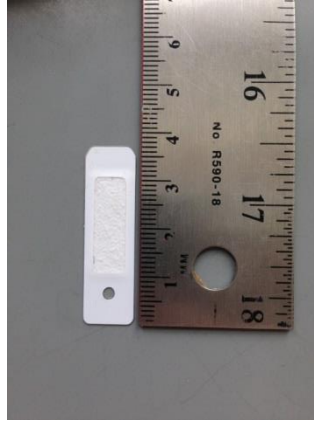
Figure 2.5. T60 Teflon-coated borosilicate glass fiber filter for the microAethalometer.
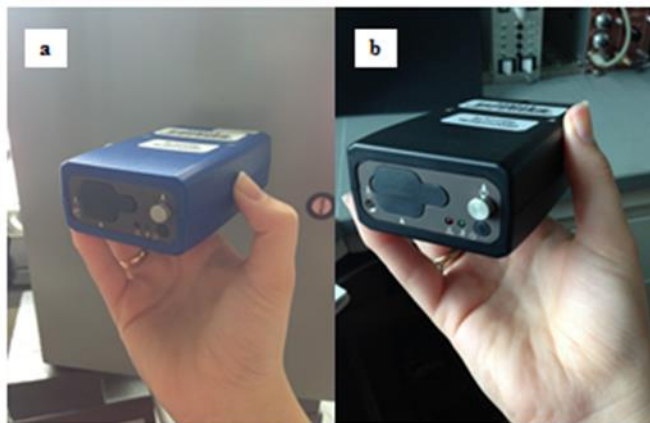
Figure 2.6. a) AE-51 microAethalometer. The AE-51 is a single wavelength instrument that records concentrations of optically absorbing particles at 880 nanometers. b) AE-52 microAethalometer. The AE-52 is a multi-wavelength instrument that measures concentrations of both absorbing and scattering particles at 880 nm and 370 nm, respectively.

Figure 2.7.   Picture of Art Mortvedt standing next to his Cessna 185 aircraft, the "Polar Pumpkin". Photo courtesy of Art Mortvedt.

2.2.2 TSI DustTrak DRX

A TSI DustTrak DRX (Figure 2.8) was also used for ground-based sampling during the small plot burns (S5-S3) of the RxCADRE campaign. The DustTrak is a handheld optical particle sizer that determines the real-time size distribution of airborne particles and mass concentrations from 0.001 mg m^{-3} to 150 mg m^{-3} in four size-segregated mass fractions: PM_1, $PM_{2.5}$, respirable (PM_4), PM_{10}, and total particulate matter fractions. The DustTrak measures based on geometric diameter, which is the true diameter of a particle (compared to the aerodynamic diameter). This instrument combines a photometric measurement to cover the mass concentration range and a single particle detection measurement to be able to size discriminate the sampled aerosol (DustTrak Theory of Operation) to obtain the size segregated mass concentrations according to the following measurements and calculations (DustTrak Theory of Operation):

(2.2) $$PM_1 = PM_{2.5} - PM_{1\text{-}2.5}$$

(2.3) $$PM_{2.5} = \text{Photometric signal multiplied by a calibration factor, which is determined from the ratio of known } PM_{2.5} \text{ mass concentrations of test aerosols (Arizona Test Dust), to the voltage response of the DustTrak.}$$

(2.4) $$\text{Respirable } (PM_4) = PM_{2.5} + PM_{2.5\text{-}4}$$

(2.5) $$PM_{10} = PM_4 + PM_{4\text{-}10}$$

(2.6) $$\text{Total Particle Matter} = PM_{10} + PM_{>10}$$

Figure 2.9 shows a schematic of the internal structure of the DustTrak DRX. The aerosol is drawn into the instrument by the diaphragm pump and passes into the sensing chamber (shown in the left diagram in Figure 2.9). The sample is then hit by a laser diode. The photo detector then picks up the signal and the signal gets separated into two different components (shown in the right diagram in Figure 2.9): single particle pulses, and photometric voltage. The voltage across the photodetector is proportional to the $PM_{2.5}$ fraction of total aerosols sampled over the wide concentration range of 0.001 mg m^{-3} to 150 mg m^{-3}. The voltage (photometric signal) is then multipled by the calibration factor from Equation 2.3. To diminish error, only particles that have an aerodynamic diameter greater than one μm are recorded. The particle mass is then calculated and recorded into the size fractions. The DustTrak weighs approximately 2.9 lbs. (1.3 kg) and had the following dimensions: 4.9 in. (12.5 cm) height x 4.8 in. (12.1 cm) width x 12.5 in. (31.6 cm) depth. The purpose for using the DustTrak during the small plot burns was to verify the amount of aerosol the microAeth was collecting and collect additional information on the size distribution of aerosols in the smoke plume.

The DustTrak DRX was also used during a Sled Dog Air Contaminant campaign, in collaboration with Dr. Todd O'Hara and his research group at the University of Alaska Fairbanks. The sampling was completed in North Pole, AK and Fairbanks, AK from December 21, 2012 to January 6, 2013. The goal of the campaign was to use the DustTrak to determine the amount of $PM_{2.5}$ the sled dogs were exposed to during the time of sampling. This campaign also allowed the researchers to observe how effective the DustTrak was at collecting air quality samples under extreme cold temperatures. Some of the days during the campaign the temperature reached -40º (-40ºC). The DustTrak was housed in a sturdy case that was bolted to a

tripod with the inlet tube for the instrument sticking out of the top of the box (Figure 2.10). The

DustTrak recorded samples every 15 minutes.

Figure 2.8. The TSI DustTrak DRX. Image courtesy of TSI Operation Manual.
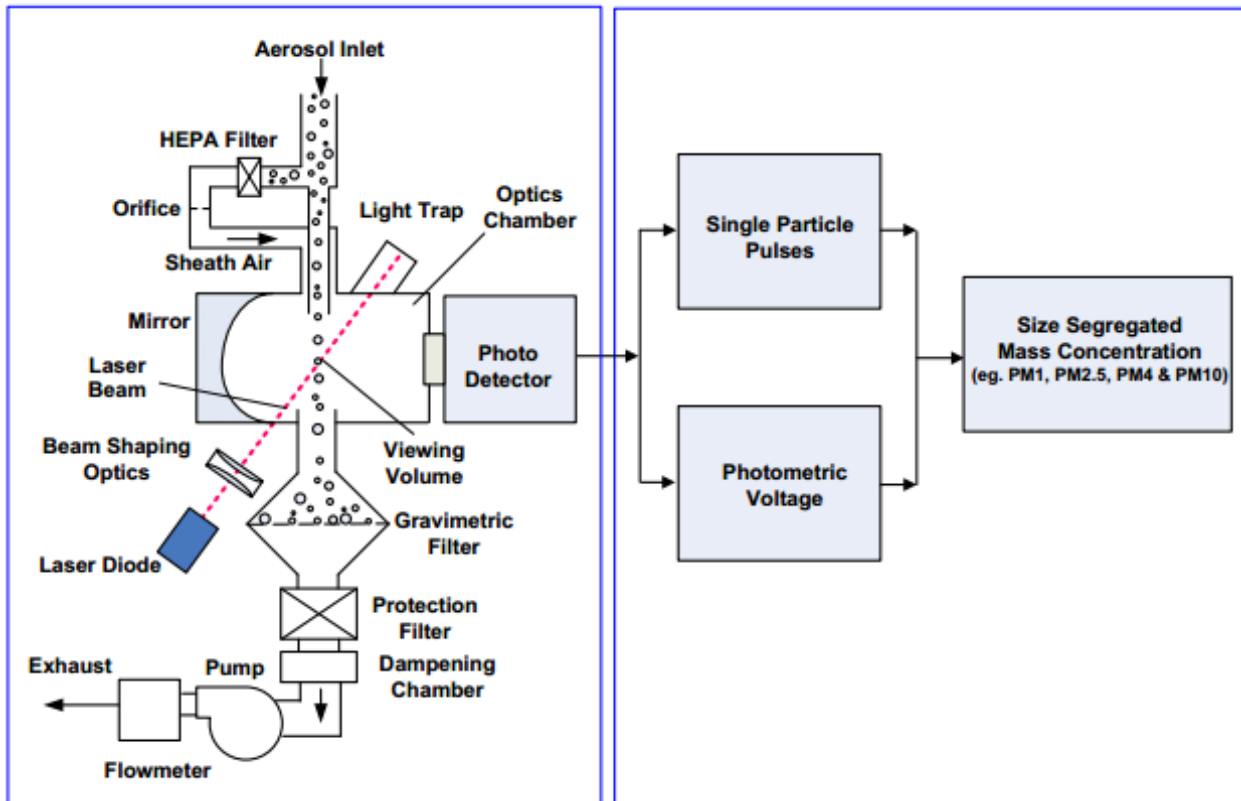
Figure 2.9.   Schematic for internal structure of TSI DustTrak DRX. Image courtesy of TSI Operation Manual.

Figure 2.10.   The instrument setup for the DustTrak during the Sled Dog Air Contaminant campaign. The inlet is outlined by the white circle.

2.2.3 Unmanned Aircraft System (UAS)

The UAS platform for the aerosol instrumentation was a Boeing ScanEagle from the University of Alaska UAS fleet. The ScanEagle (Figure 2.11) is an autonomous, gasoline-fueled aircraft that is launched from a trailer mounted, Mark 4 launcher (Figure 2.11), and is typically used for surveillance purposes. The ScanEagle has the following dimensions: 5.1 ft. (1.55 m) length x 10.2 ft. (3.11 m) width (wingspan). This UAS is very agile and can weigh between 30.9 lb. (14 kg) (empty structure) and 48.5 lb. (22 kg) (max takeoff weight). The ScanEagle can fly for over 24 hours and up to 19,500 feet (5,950 m) in altitude. The maximum horizontal speed is 80 knots but typical cruise speeds are between 50 and 60 knots (25.7 m/s and 30.9 m/s, respectively).

Figure 2.11. Boeing ScanEagle ready for takeoff on a Mark 4 launcher.

2.3 The RxCADRE Experiment

Between October 31st and November 6th 2012, scientists from the University of Alaska Fairbanks used ground-based instrumentation to collect aerosols in the plumes created by four different prescribed burns during the RxCADRE experiment, three small plots and one large plot. Aerosols from the small plot burns were only collected by ground-based sensors due to the short duration of the burn and the high flight altitude (500 meters) of the UAF Boeing ScanEagle, which was above the low smoke plume (less than 500 meters). However, the large-plot burn at RxCADRE provided the opportunity to integrate and fly the first Aethlabs microAethalometer on a UAS. The goal of the UAF aerosol team's experiment was to have a successful integration of the microAethalometer on a Boeing ScanEagle. The integration would allow for the airborne, real-time sampling of black carbon in smoke plumes from wild and prescribed fires.

The two-wavelength microAeth (AE-52) and the DustTrak DRX, mounted on a 1.3 m ladder (Figure 2.12), collected smoke absorption data for the three small-burn plots (S5, S4, and S3), during the RxCADRE campaign, on November 1st, 2012 (Figures 2.2 and 2.3). The ladder was positioned in the expected paths of the smoke plumes from each fire. The AE-52 was set to collect samples every 60 seconds (time base), with a flow rate of 100 milliliters per minute (ml min^{-1}). The DustTrak DRX collected samples every 15 seconds with a flow rate of one liter per minute (L min^{-1}). The DRX has a flow rate limitation and the range could only be adjusted from one L min^{-1} to four L min^{-1}.

Researchers at the University of Alaska Fairbanks were successful in mounting the single-wavelength microAeth (AE-51) onto a Boeing ScanEagle aircraft, Figure 2.11, for the

large plot burn (plot B-70), during the RxCADRE campaign, on November 2nd, 2012. The microAeth was placed in the back of the fuselage in front of the fuel compartment. The inlet tube for the instrument stuck 1.3 cm out of the bottom of the aircraft and created a straight path from outside the airframe into the instrument. The AE-51 was set to collect samples every one second with a flow rate of 50 ml min^{-1}. In order to make sure the instrument was recording data when the ScanEagle impacted the plume, the sampling rate had to be shortened to one second per sample, compared to one minute per sample for the ground-based AE-52.

Figure 2.12. Image of the instrument set up for the small plot burns during the RxCADRE
campaign.

2.4 Laboratory Experiments

2.4.1 Aerosol Generator

Aerosols of known composition, black carbon (bone carbon) and sodium chloride (NaCl), and size were generated to confirm the size of the aerosols entering the two microAethalometers (AE-51 and AE-52) as well as the DustTrak. These aerosols also were used to test the response times of the instruments varied.

The aerosol generator used to create the aerosols was a TSI Model 3074B Filtered Air Supply attached to a TSI Model 3076 Constant Output Atomizer. The aerosol starts out in a liquid solution in the atomizer. Clean air passes through the atomizer and sucks solution into the atomizing chamber where the solution is broken into multiple small droplets by a nozzle with a strong airflow through it. Small droplets follow the airflow around a 90-degree angle while larger droplets impact the wall of the chamber and fall back into the solution reservoir. The aerosol then passes through the liquid droplet trap to remove any large droplets that remain in the airstream and into a TSI Model 3062 Diffusion Dryer. It was important the aerosol was dried prior to entering the microAethalometer because the microAeth had no tolerance for moisture in the inlet chamber. From the dryer, the aerosol passes through the TSI Kr-85 Isotope neutralizer before going into the instrument. According to the TSI Particle Technology Catalog, the particles generated by the instrument are in the size range of 0.01 μm to 2.5 μm. Figure 2.13 shows a schematic of the set-up of the aerosol generator.
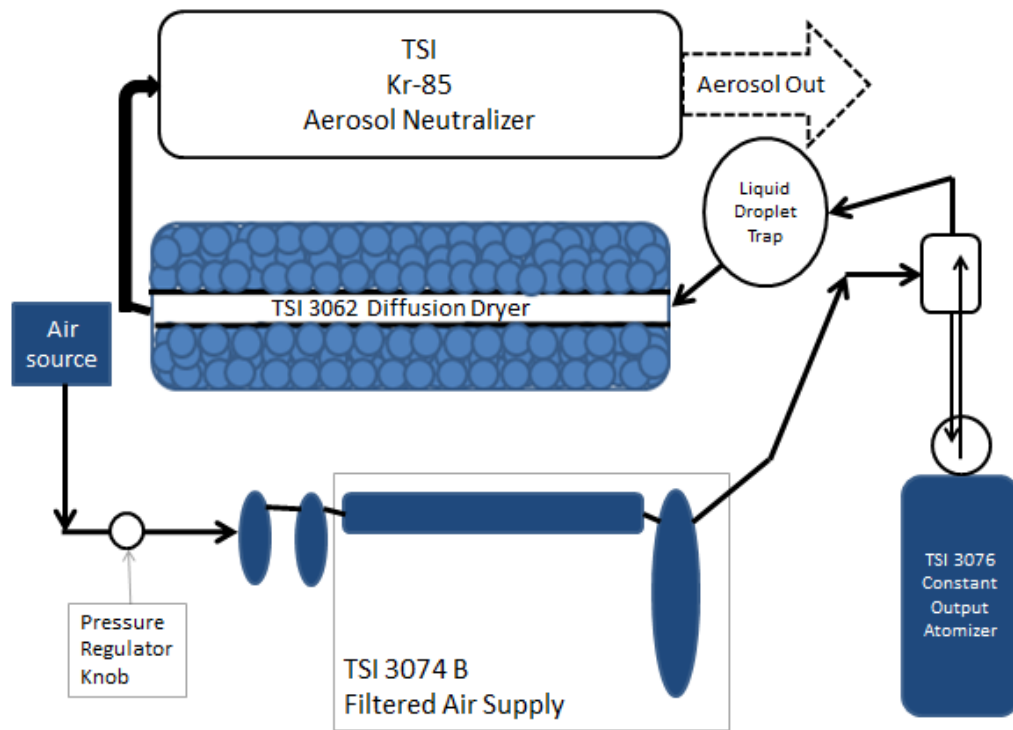
Figure 2.13. Schematic of the TSI aerosol generator set up.

2.4.2 Optical Particle Sizer

In addition to the DustTrak another optical particle sizer (OPS) was used in the laboratory experiments to determine how accurate the microAeths and DustTrak were in the collection of aerosols. The Model 3330 OPS was also manufactured by TSI and the internal structure is similar to the DustTrak in Figure 2.9. Running the OPS alongside the microAeth allowed for the observation of how many particles of specific sizes were making it into the instruments.

The optical particle sizer has a wide range of adjustable size channels (also referred to as bins) available. There are a maximum of sixteen bins available for the instrument and the size ranges measure from 0.3 μm to 10 μm. Because the microAeth only records particles with a diameter of 2.5 μm or lower, the number of bins in the OPS was adjusted from sixteen to eleven. The upper cut-off points for each of the eleven bins were as follows:

Bin 1: 0.300 μm
Bin 2: 0.374 μm
Bin 3: 0.465 μm
Bin 4: 0.579 μm
Bin 5: 0.721 μm
Bin 6: 0.897 μm
Bin 7: 1.117 μm
Bin 8: 1.391 μm
Bin 9: 1.732 μm
Bin 10: 2.156 μm
Bin 11: 2.685 μm

The OPS provides an output of number of particles per sample. In order to compare the OPS data with the microAeth data, several conversions needed to be done to start from particle per sample and end up with mass concentration. For the comparison the OPS was set to record data every ten seconds until it reached 500 samples. The first conversion needed to get the OPS data to mass concentrations is to convert the OPS data from particles per second to particles per

cubic centimeter (cm^{-3}). To do this conversion, the flow rate of the OPS (16.67 cm^3 s^{-1}) was multiplied by the length of each sample (ten seconds), to get a new flow rate that accounts for the entire sample (166.7cm^3 for every ten second sample). Then, the number of particles per each sample was divided by the new flow rate (166.7 cm^3), which gave the particle concentration for each sample in each of the eleven bins of the OPS (cm^{-3}). The particle concentration limit for the OPS is 3,000 cm^{-3}.

The volume of a sphere multiplied by the density of black carbon (1.8 g cm^{-3}), Equation 2.7, was used to determine the mass of an individual spherical particle of a known radius in grams. The median of the size range for each bin was used as the radius in Equation 2.7.

(2.7) $$m = \frac{4}{3}\pi r^3 x \, \rho$$

Multiplying the particle concentration (# cm^{-3}) by the product of Equation 2.7, gives the mass per volume (g cm^{-3}) for each sample in each bin (Equation 2.8).

(2.8) $$\frac{particle}{volume} x \frac{mass}{particle} = \frac{mass}{volume}$$

The last conversion (Equation 2.9) is the dimensional analysis needed to convert the result of Equation 2.8 from g cm^{-3} to ng m^{-3} and give the mass concentration in the desired units.

(2.9) $$\left(\frac{1g}{cm^3}\right) x \left(\frac{10^9 ng}{1g}\right) x \frac{(100 \, cm)^3}{1m^3} = \left(\frac{ng}{m^3}\right)$$

2.2.3 Characterization of the microAethalometer

To fully understand the microAeths, tests were conducted in the laboratory to characterize the instruments. The AE-51 and AE-52 have different parameters for the time base but have the same flow rate options. The flow rates for the instruments were set identically for

the laboratory tests to facilitate determining if the instruments' sensitivity to aerosols was the same for the two instruments.

The parameters that were tested for both the AE-51 and AE-52 are listed below:

- Response time of the instrument

- Detection limit of the instrument

- Limitations of the instruments' software

It was important to determine if there was a difference in the response times of the instruments to different aerosols (i.e. whether the aerosol had absorbing properties [black carbon] or scattering properties [sodium chloride]) and different aerosol concentrations. It was also important to learn how much time was needed for the instruments to stabilize after start up. This information was needed to verify the quoted detection limits of the instruments and response times.

To test the parameters above, a series of box tests were performed in the laboratory. Figure 2.14 shows a diagram of how the box test was set up for the experiment. The aerosols were dispersed from the aerosol generator into a small cardboard box. The box was completely sealed to make sure the same air was entering every instrument. The inlet tubes of the microAeths and the OPS were attached to the opposite end of the box from the aerosol generator outlet. The aerosols used in the testing were black carbon, which has absorbing properties, and sodium chloride, which has scattering properties. Both aerosols were used in concentrations of 0.15 grams per liter (g L^{-1}) and 0.50 g L^{-1}. The concentrations were chosen at random to help characterize the instruments.
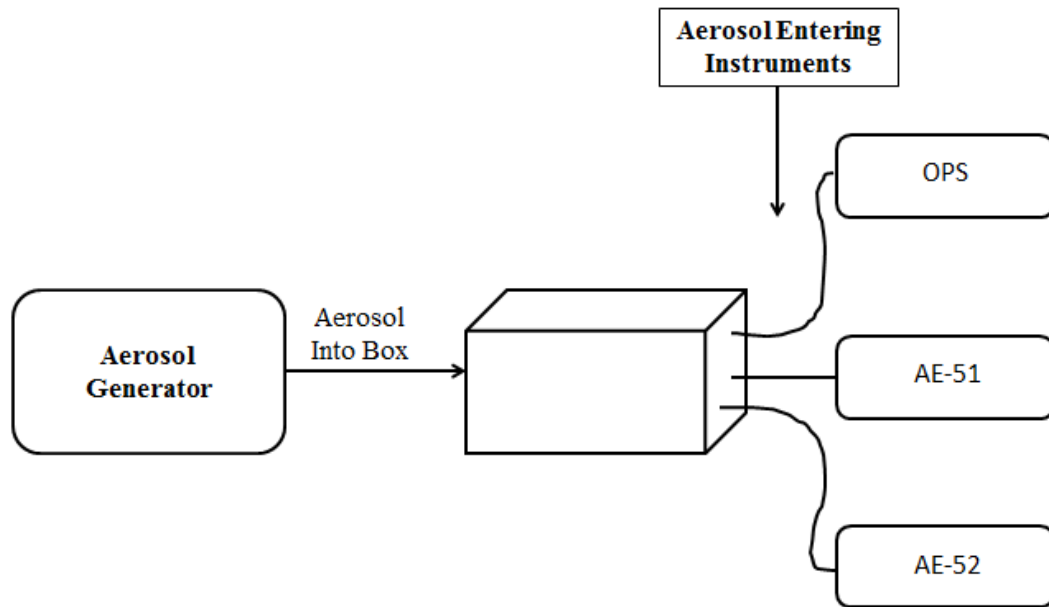
Figure 2.14. Schematic of how the box test experiments were completed.

For the 0.15 g L^{-1} black carbon box tests, all four instruments were tested; the AE-51, AE-52, the OPS and the DustTrak DRX. The AE-51 and AE-52 were both set to record samples every sixty seconds at fifty ml min^{-1}. The OPS recorded data every minute as well, and the DRX recorded data every ten seconds. For the 0.50 g L^{-1} black carbon box tests the AE-51, AE-52, and the OPS were tested. The AE-51 and AE-52 were both set to record samples every sixty seconds at fifty milliliters per minute. The OPS recorded data every ten seconds.

Before the NaCl box test was started, the aerosol generator purged the remaining black carbon aerosols by pumping deionized water through the instrument. A new cardboard box was used for the NaCl tests. During the 0.15 g L^{-1} sodium chloride box tests the AE-52 and the OPS were tested. The AE-52 was set to have a flow rate of fifty ml min^{-1} and recorded data every ten seconds. The OPS recorded data every ten seconds as well. For the 0.50 g L^{-1} NaCl box tests the AE-52 and the OPS were tested. The AE-52 had the exact same flow rate and time base as the 0.15 g L^{-1} NaCl box test and the OPS did as well.

The two microAeths and the OPS were used during two small fires in the fume hood of the Cahill lab (Figure 2.15). The fuel source for the fires was paper birch. Paper birch was used because it is a common fuel in boreal forest fires. The lab fires were conducted in order to see how the instruments respond to high concentrations of black carbon aerosols. For both fires, the AE-51 was set to record data every second at a flow rate of 50 mlpm and the AE-52 was recording data every ten seconds with a flow rate of 50 mlpm. The OPS was set to record data every ten seconds.

Characterizing the two microAethalometers was important because future work will benefit from the information the instruments provide during the laboratory experiments. The long term

goal would be for the two microAeths to be used for research on multiple types of unmanned aircraft, not just the Boeing ScanEagle.

Figure 2.15. Image of the second lab fire in the fume-hood of Dr. Catherine Cahill's laboratory.

The fire was started by lighting copier paper on fire and letting the paper birch logs catch on fire.

Chapter 3 – Results and Discussion

3.1 RxCADRE

During the RxCADRE campaign, the multi-wavelength microAeth (AE-52) and the DustTrak collected aerosol samples during the small plot burns (S5, S4, S3) from the top of a 1.3 meter ladder positioned in the expected paths of the smoke plumes for each fire. However, due to the variability of the winds, the instruments were not in the center of the plume for all three small plot fires. The ladder was moved between the S5 and S4 fires, fires 1 and 2 respectively, to maximize the smoke collected by the instruments. During the S4 fire, oversaturation was reached, as indicated by the arrow in Figure 3.1. After oversaturation occurs, the instrument only responds to large changes in aerosol concentrations impacting the filter. Minimal data was collected from fire S3 because the wind blew most of the smoke plume to the west of the microAeth, not because the sampler was oversaturated.

During the fires, there is a larger signal in the 370 nm wavelength (UVPM) of the microAeth than the 880 nm wavelength (BC) because the smoke plume contained many light-scattering particles in addition to the highly absorbing black carbon particles. The observed peak height difference between the two wavelengths therefore correlates to how many aromatic organic species there are in the sample as well as some scattering aerosols like sulfates. This result implies that over half of the particulate matter in the smoke plume is organic matter produced by the incomplete combustion of the fires' fuels.

Figure 3.2 shows the results the DustTrak collected during the three small plot burns. TSI calls PM_4 the respiratory (RESP) size fraction. The same pattern is observed, as in Figure 3.1, but the concentrations vary because: PM_{10} includes PM_4 and all particulate matter between 4 and

10 microns in diameter, PM_4 includes $PM_{2.5}$ and all particulate matter between 2.5 and 4 microns in diameter, and $PM_{2.5}$ includes PM_1 and all particulate matter between 1 and 2.5 microns in diameter. The same pattern and peak concentration occurs in each size fraction shown in Figure 3.2. The consistent height of the peaks indicates that all of the collected particulates are in the PM_1 size fraction range, which is consistent with a nearby high-temperature combustion source. Another important feature of Figure 3.2 is that the concentrations recorded in µg m^{-3} are much higher than in Figure 3.1. Because BC is only a fraction of the particulate mass from combustion processes, one would expect the BC mass to be less than that of light scattering particles. Another reason for the microAeth recording a lower value than the DustTrak is particle shadowing. Particle shadowing occurs when particles start stacking on top of one another on the filter strip as the strip starts to overload. The light the particle landing on top of another particle would otherwise absorb is blocked by the particle under it; therefore, the light passing through the filter is not attenuated by the new particle and it is not counted towards the concentration. Particle shadowing could result in the microAeth becoming oversaturated at 600 µg m^{-3} (Figure 3.1) whereas the DustTrak was able to record concentrations up to 2,000 µg m^{-3} (Figure 3.2). It is also possible that the microAeth is underestimating the amount of particulate matter generated by the fire.
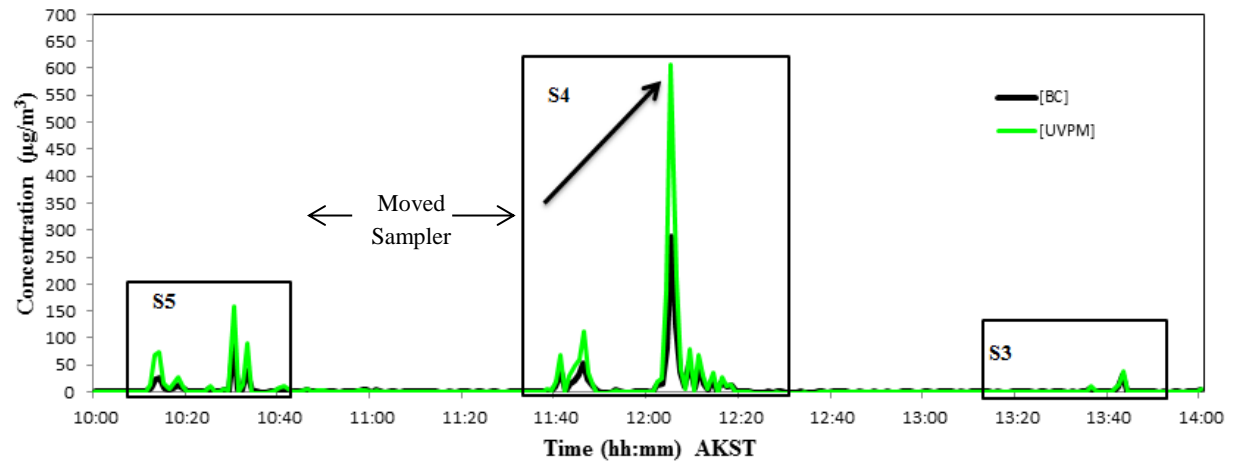
Figure 3.1. Results from small plot burns at RxCADRE. The arrow indicates the point of oversaturation.
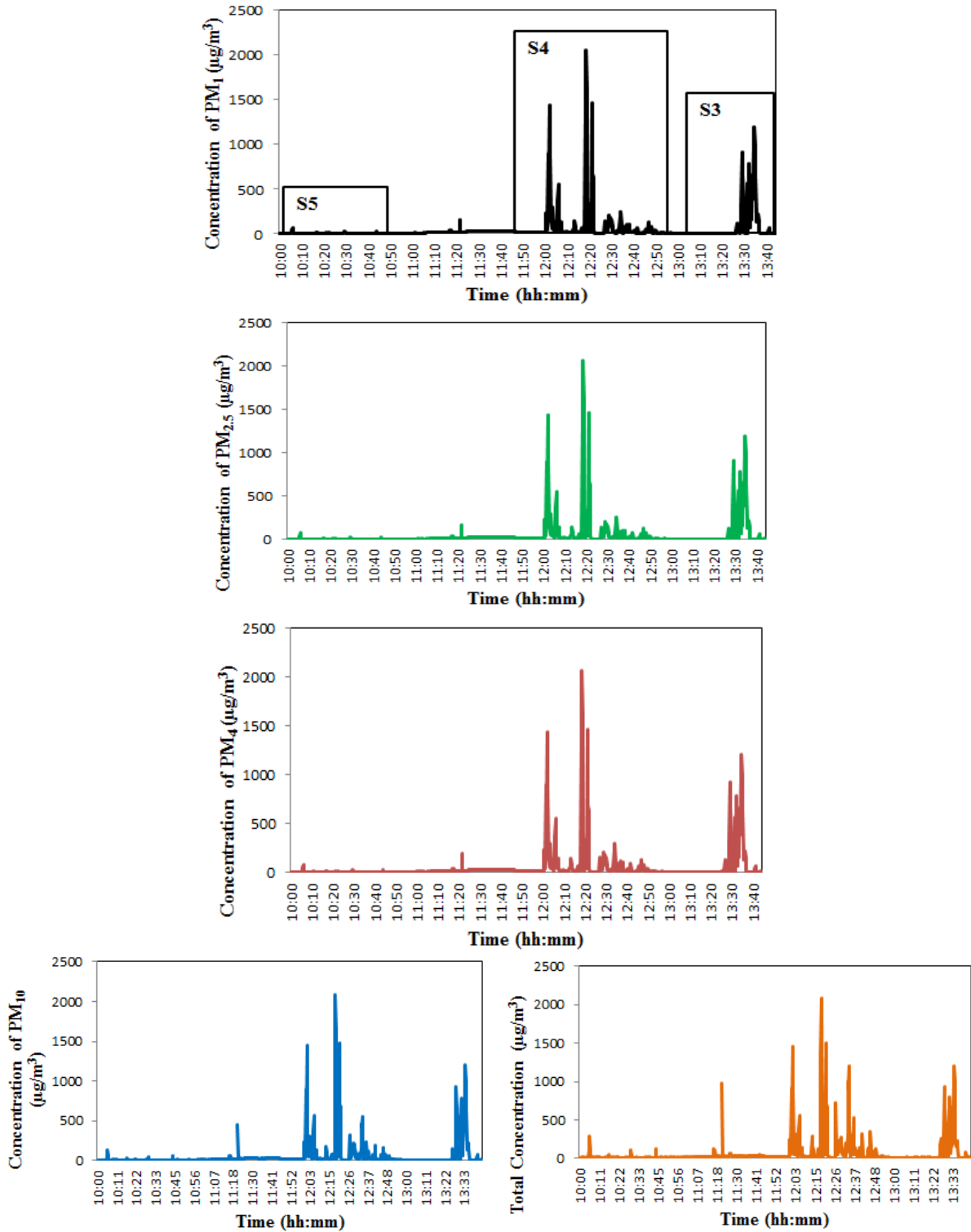
Figure 3.2. Results for the DustTrak DRX from the RxCADRE campaign. The time scale was from 10:00 am AKST to 14:00 AKST.

Figure 3.3 shows the placement of the microAeth (AE-51) in the fuselage compartment of the Boeing ScanEagle. The AE-51 was positioned in the back of the fuselage and held in place by Velcro. Weight and balance adjustments were made by one of the ScanEagle flight engineers, Peter Elstner, after the integration.

Figure 3.4 shows the position of the inlet tube for the AE-51. The inlet tube stuck out of the bottom of the fuselage through a hole where an extra screw was used on the aircraft. The inlet only extended 1.3 cm from the fuselage to minimize the effect the wind would have on the shape and orientation of the inlet tube.

The Boeing ScanEagle was launched at 5:40 am AKST and flown just under 9 kilometers to the region of the large plot burn. The ScanEagle flew in a circular pattern at 500 m in altitude above the prescribed burn to observe the burn and its smoke plume from 360 degrees around the fire. The aircraft orbited for five and a half hours until the prescribed burn was completed and then the aircraft returned to base to land at 11:30 AKST.

Figure 3.3. Image showing the placement of the AE-51 microAethalometer in the fuselage of the

Boeing ScanEagle.

Figure 3.4. Boeing ScanEagle with AE-51 microAethalometer onboard. The white circle shows

the inlet tube of the microAeth sticking out of the bottom of the aircraft.

Figure 3.5 shows the concentration of black carbon aerosols collected by the microAeth, AE-51; during the flight over the large plot burn (Figure 2.4). The fact that aerosols were collected showed that the scientists from the University of Alaska Fairbanks were successful in the first integration of an Aethlabs microAethalometer on an unmanned aircraft, the Boeing ScanEagle.

The smoke plume reached the ScanEagle altitude, of 500 m (Figure 3.6) at 10:04 AKST as shown by the increase in black carbon aerosol concentration in Figure 3.5. The magnitude of the peaks in Figure 3.5 are smaller than in Figures 3.1 and 3.2 because for the small plot burns the microAeth was ground-based, right in the line of the smoke for the majority of the burns. During the large burn (Figure 3.5), the smoke was mostly below the instrument as the ScanEagle was orbiting the plot. The peaks at 5:38 am and 11:15 am AKST in Figure 3.5 are the result of exhaust and generator emissions at the unmanned aircraft staging platform.
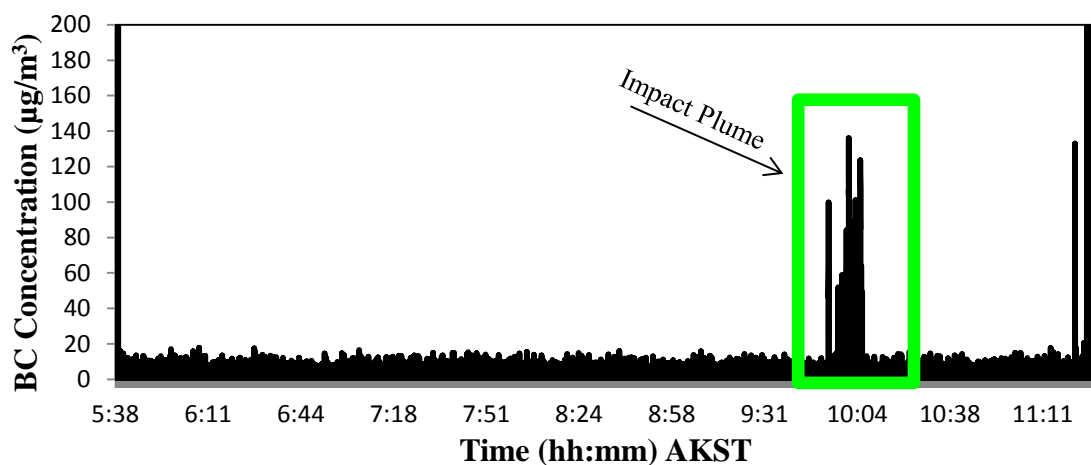
Figure 3.5. Results from the large plot burn during the RxCADRE campaign. The smoke plume

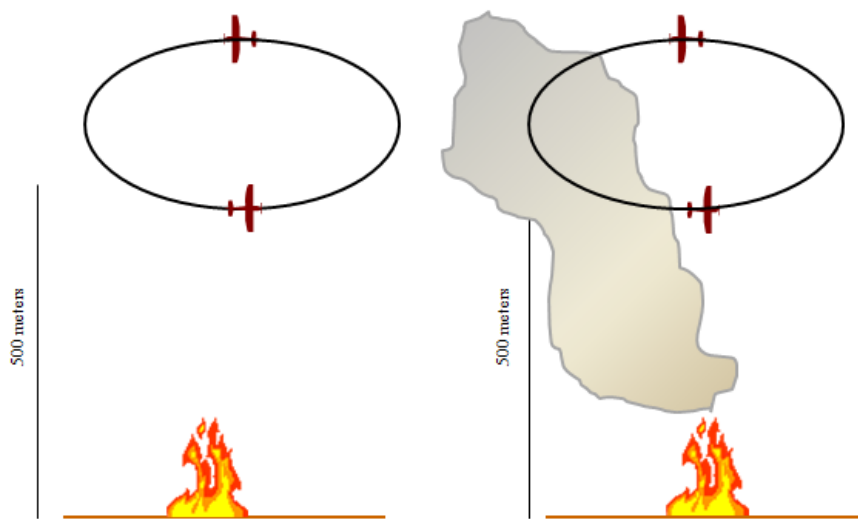reached the aircraft at 10:04 AKST as indicated by the green box on the graph.

Figure 3.6. Schematic of flight path at the beginning of the plot burn (left) and during plume

impact (right).

Both microAethalometers were also flown, on a solo flight by pilot Art Mortvedt, to the geographical North Pole on the Polar Pumpkin (Figure 2.7), a Cessna 185, from March 2013 to May 2013. The purpose of the flight was to sample airborne black carbon between Fairbanks and the North Pole. The researchers involved were also hoping to observe the effectiveness of the microAeths in high wind conditions as well as extreme cold climates. The microAethalometers had many complications during the flight. Mr. Mortvedt encountered multiple failure modes as well as battery power challenges due to cold temperatures. The cockpit was not heated so the temperature inside the cockpit was closer to ambient air temperature.

Mr. Mortvedt was able to collect aerosol samples on his last two legs of the trip. Figure 3.7 shows the AE-52 (multi-wavelength) data that was collected from Norman Wells to Inuvik, both in the Northwest Territories. The AE-52 was set to a flow rate of 100 ml min^{-1} and data was recorded every one minute. Figure 3.8 shows the AE-51 (one wavelength) data that was collected from Inuvik, Northwest Territories, to Old Crow, Yukon Territory, to Fairbanks, AK. The AE-51 was set to a flow rate of 150 ml min^{-1} and data was recorded every one second. The data in both Figures 3.7 and 3.8 were collected by removing the inlet tube from the microAeths, and placing the instruments in the cockpit, near an open aircraft fresh air vent. Because the black carbon concentrations were so high (up to 350 µg m^{-3} in Figure 3.8) for Mr. Mortvedt's final flight of the trip, it was assumed that the aerosols collected were compromised due to emissions from the engine of the aircraft, and the black carbon aerosols were not from the atmosphere.

After the trip was completed, the researchers determined the flow rate was not set fast enough to counter-act the amount of air that was being forced into the inlet chamber (i.e. there was excessive ram air pressure), while the instrument and plane were airborne. This study

showed that the microAeths are very sensitive in high winds, and microAeth inlets must be placed so the effects of ram air are minimized.
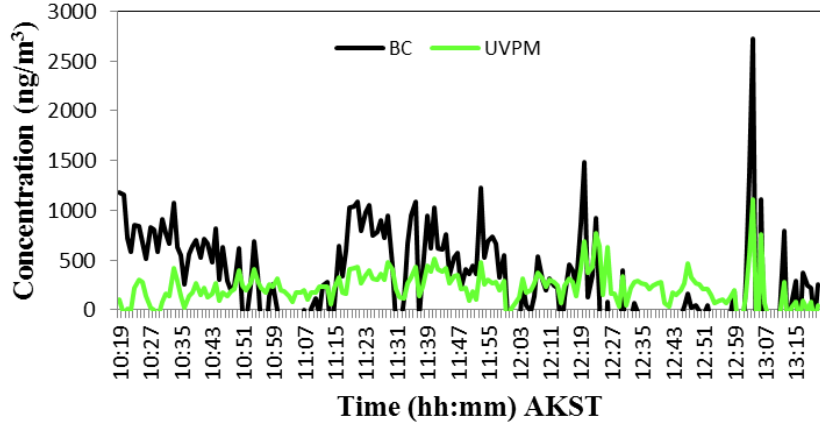
Figure 3.7. Data from the multi-wavelength aethalometer collected between Norman Wells and Inuvik, Northwest Territories.
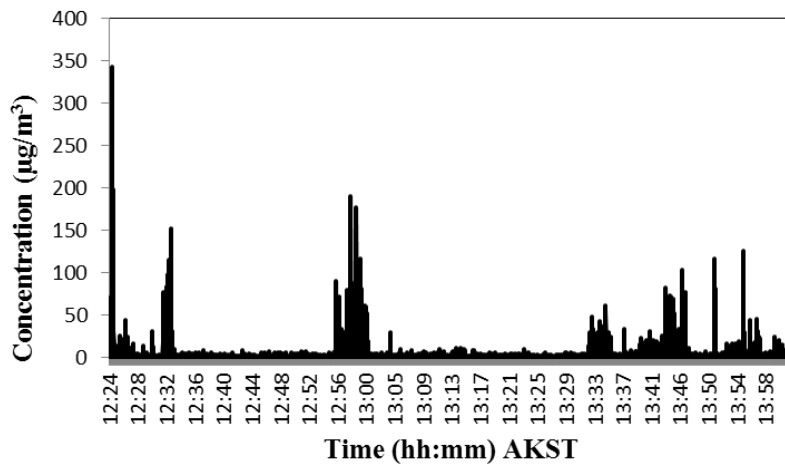
Figure 3.8. Data from the single wavelength aethalometer collected between Inuvik, Northwest Territories, Old Crow, Yukon Territories, and Fairbanks, Alaska.

The AE-52 microAeth was also used to collect smoke aerosols from the Nenana Fire which burned over 80 acres of white spruce in June 2013. Figure 3.9 shows the data collected by the AE-52 when the smoke plume reached Fairbanks. Shortly after sampling was initiated at 13:30 AKST, the concentrations of both UVPM and BC were high at approximately 15:00 AKST (18,000 ng m^{-3} UVPM concentration and approximately 7,000 ng m^{-3} BC concentration). After approximately two hours of sampling, the concentrations started to gradually decrease, until 19:30 AKST where the concentrations appear to level out and remain relatively constant for the rest of the day. This behavior is consistent with the center of the smoke plume shifting further away from the instrument setup.

Figure 3.9. Data collected by the AE-52 in Fairbanks during the Nenana Fire in Alaska.

From December 21, 2012 to January 7, 2013, researchers from the University of Alaska Fairbanks took part in a Sled Dog Air Contaminant campaign. Graduate students from Dr. Todd O'Hara's laboratory worked with Dr. Catherine Cahill's graduate students. During the period of sampling,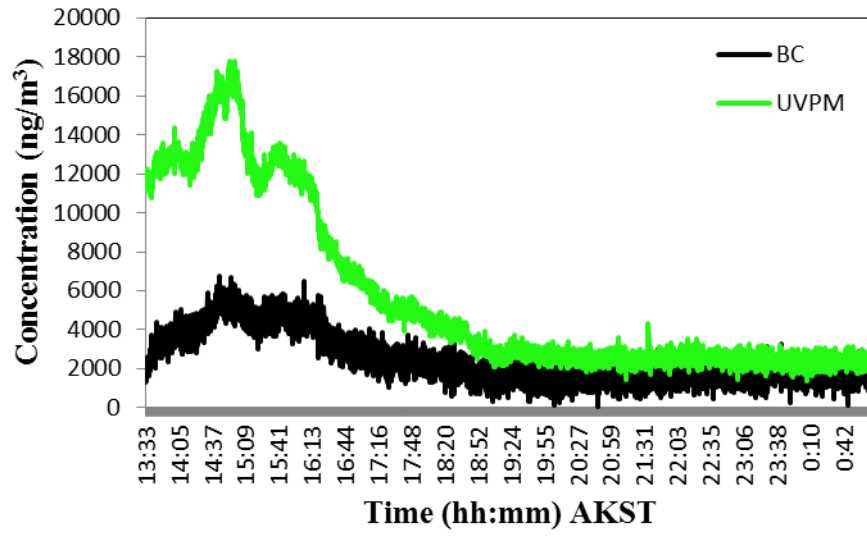 temperatures reached -40ºF (-40ºC). The sampling took place at two kennels, the first in Fairbanks, AK, and the second in North Pole, AK. Figure 3.10 shows the results from the sled dog air contaminant campaign.

It was found that the sled dogs were exposed to very high concentrations of $PM_{2.5}$. The Environmental Protection Agency (EPA) sets the ambient air quality standard for, $PM_{2.5}$, at 35 micrograms per cubic meter of air ($\mu g\ m^{-3}$) averaged over 24 hours. As Figure 3.10 shows, the dogs were exposed to concentrations as high as 550 $\mu g\ m^{-3}$ in Fairbanks and 620 $\mu g\ m^{-3}$ in North Pole. The high concentrations of $PM_{2.5}$ are credited to the temperature inversion that is a stable meteorological feature during winter in Fairbanks and North Pole. The inversion provides a layer of stable air over the cities that traps particles generated by local sources under it, causing increased concentrations of $PM_{2.5}$ under the inversion layer. In February 2007 there was a difference in temperature from 44º in Fairbanks, AK to -2º in Chatanika, AK. Since Fairbanks sits at a higher elevation, above the inversion, the weather is typically warmer than other places (FAI) in Fairbanks.
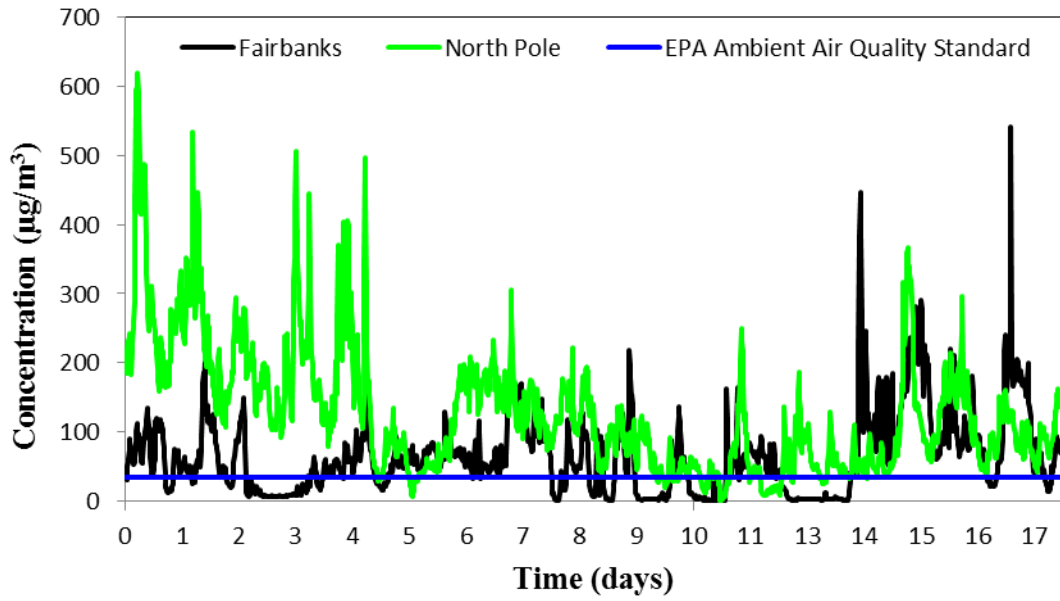
Figure 3.10. Results from the Sled Dog Air Contaminant campaign from December 21, 2012 to January 7, 2013.

3.2 Laboratory Experiments

3.2.1 Characterization of microAethalometer

In order to test the response times of the microAeths and optical particle counters, aerosols of known concentrations and compositions were created using a TSI aerosol generator and sucked into the instruments. The aerosols chosen for the experiment were black carbon (bone carbon) and sodium chloride (NaCl). Black carbon was chosen because BC is optically absorbing, whereas NaCl was chosen because it has optical scattering properties. However, bone carbon is not pure BC, so the resulting aerosol will have a scattering component. Two solution concentrations were used to generate aerosols for the laboratory tests: 0.15 g L^{-1} and 0.5 g L^{-1}.

After turning on the microAethalometer, the internal pump needs to reach the flow rate designated by the software before any sampling begins. Both microAethalometers used MicroAethCOM software, designed by Magee Scientific. The device settings for the flow rates were the same for both the AE-51 and the AE-52. The flow rate is measured in milliliters per minute (mL min^{-1}) and was set to 50 mL min^{-1}. It was found that the AE-51 microAeth takes on average forty-five seconds to start up, and the AE-52 takes on average twenty-five seconds before sampling begins. The instruments recorded samples every 60 seconds as well.

Box tests (Figure 2.13) were used to carry out most of the laboratory experiments. The box tests to determine the instruments' responses to black carbon aerosols were conducted first. Both of the microAeths, the OPS, and the DustTrak were tested while the concentration of the bone carbon was 0.15 g L^{-1}. Figure 3.11 shows the results from both microAethalometers during the 0.15 g L^{-1} BC box tests. These results are the average concentrations recorded by the instruments from six trials. The microAeths were started at the same time the aerosol generator

was turned on. The higher concentrations of UVPM might be due to the aerosol generator not being purged prior to the tests (i.e. there may have been some scattering aerosols present in the generator system before the experiment started). Figure 3.11 shows that the black carbon channels for both the AE-51 and AE-52 are in sync with one another and both are recognizing BC at similar concentrations.

Figure 3.12 shows the average results from the DustTrak, OPS, and both microAeths for the 0.15 g L^{-1} BC box test trials in August 2014. The DustTrak was started prior to the aerosol generator, and a large increase in aerosol concentration can be seen shortly after the instrument started, in Figure 3.12, where it is assumed the aerosols started entering the inlet chamber of the DustTrak.

It is important to point out that the DustTrak and OPS recorded a much higher concentration of aerosols than both of the microAethalometers. This observation confirms the results from the RxCADRE campaign, showing the microAeths underestimate the amount of aerosol being collected because they do not measure non-organic scattering aerosols, only absorbing ones. If the results from the OPS (Figure 3.12) are compared to the results from the microAeths (Figure 3.11), the aerosol concentrations collected by the microAeths are lower than those collected from the OPS-again giving confirmation to the above statement that the AE-51 and AE-52 are underestimating the aerosol concentration. The flow rate difference between the microAeths (50 ml min^{-1}) and the optical particle sizers (1 L min^{-1}) were accounted for in the calculations (Equations 2.7 through 2.9) but rounding errors could contribute slightly to the difference in concentrations.
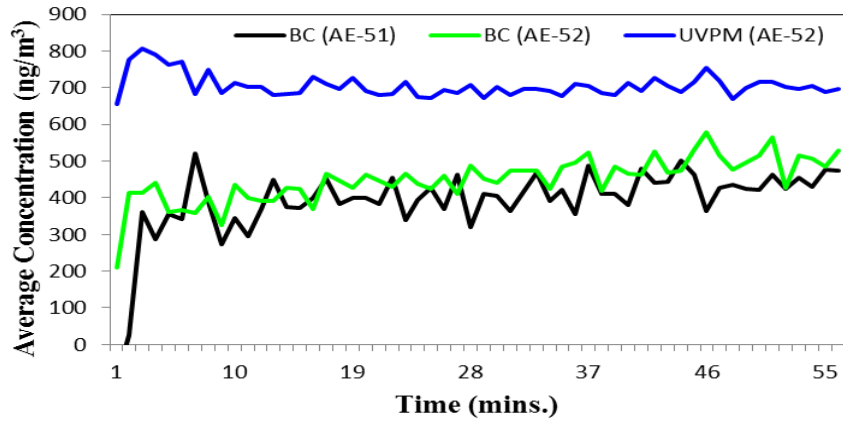
Figure 3.11. Average results from the AE-51 and AE-52 during the six 0.15 g L^{-1} black carbon
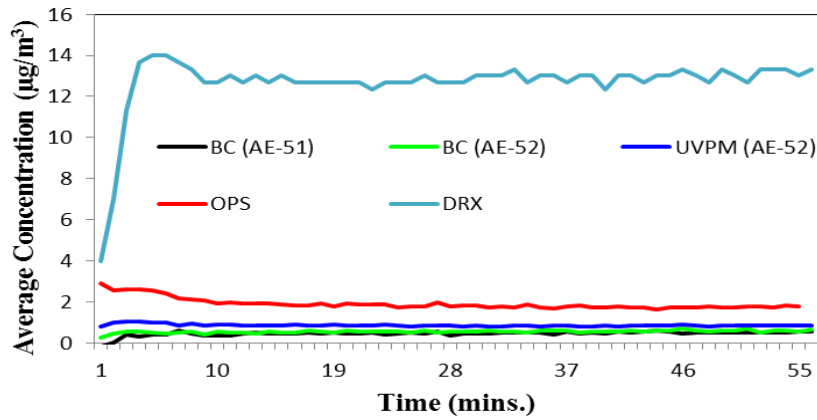
box tests.

Figure 3.12. Results from the DustTrak, OPS, and both microAeths during the box test with the

black carbon concentration set to 0.15 g L^{-1}. These results are from the month of August.

The next set of box test experiments were done with a black carbon aerosol concentration of 0.50 g L^{-1}. The DustTrak, OPS, and both microAeths were used in these experiments as well. Figure 3.13 shows the average concentration recorded by both microAethalometers over the course of 8 trials. The DustTrak results (Figure 3.14) showed that the concentration of aerosols collected in the $PM_{2.5}$ size fraction were much higher (recorded in µg m^{-3}) compared to the other instruments. The OPS results (Figure 3.14) showed the concentrations were lower than both of the microAeths as well as the DustTrak. The low concentration recorded by the OPS is potentially the result of inlet placement during the experiments. There was no fan in the box so the mixing of aerosols may not have been very good. Also, the aerosol flow may have been directed at the other instruments better than the OPS. The results from the DustTrak confirm that the microAeths are still underestimating the concentrations of aerosols. The DustTrak and OPS were both calibrated for aerosols with a 1.8 g cm^{-3} density, which is the density of BC. The AE-51 and AE-52 record very similar concentrations for the black carbon aerosols. Since the microAeths assume all absorbing particulates in the 880 nm channel are black carbon, the other species that absorb at 880 nm that are not BC cause the assumption made by the instruments to underestimate the number of particles that are actually present. These results again show the good agreement between the microAeths during the 0.15 g L^{-1} aerosol concentration tests (Figure 3.11). This proves that the BC aerosols concentration should record the same for both instruments regardless of the solution concentration. Figure 3.15 shows the breakdown of the average number of particles that entered the OPS by size during both BC box experiments. It is clear that the aerosol generator only produces submicron particulates.
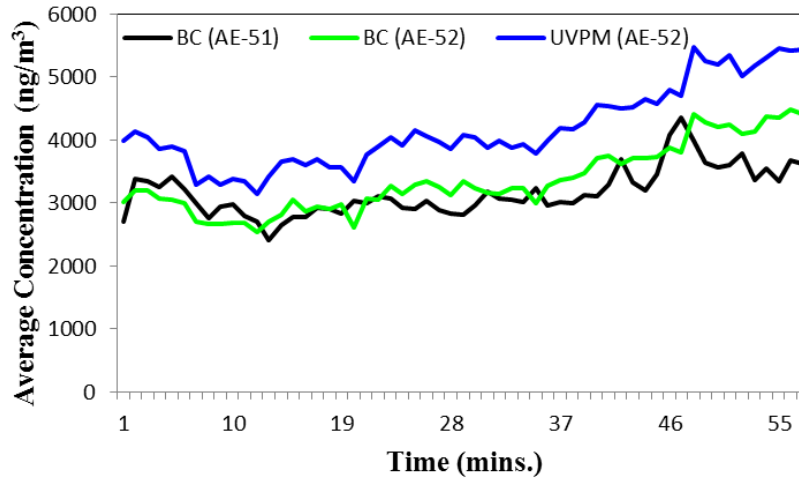
Figure 3.13. Average results from both microAeths during the eight 0.50 g L^{-1} BC concentration box tests.
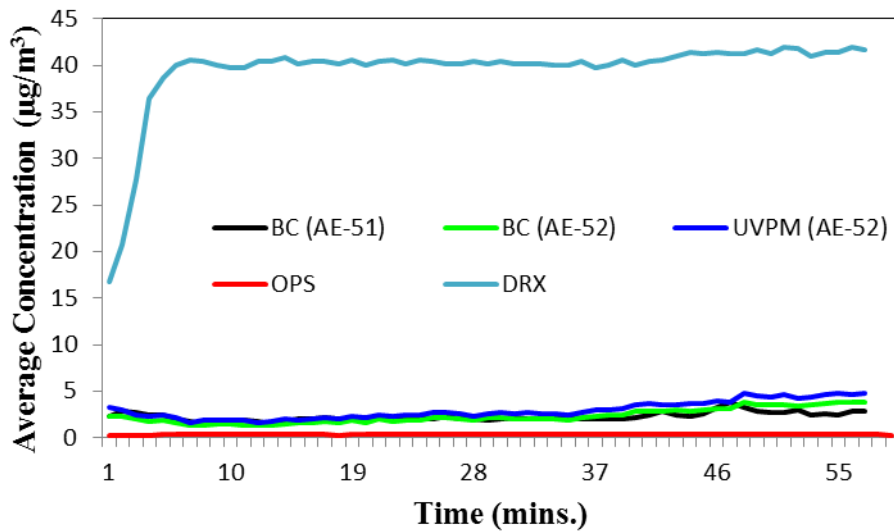

Figure 3.14 Results from the DustTrak, OPS, and both microAeths during the 0.50 g L^{-1} BC concentration box tests from August.
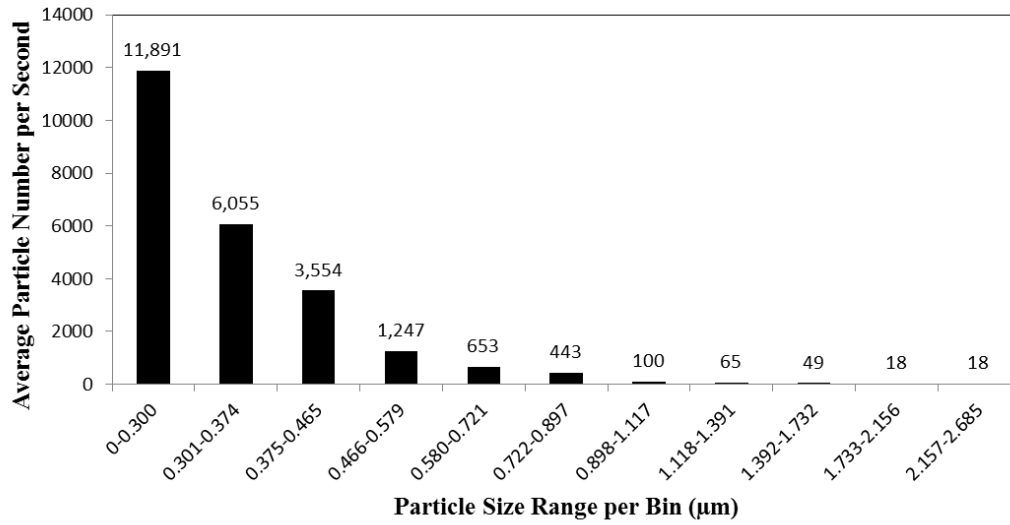
Figure 3.15. The breakdown of the average number of particles per bin in the OPS during the BC box test.

The next group of laboratory experiments dealt with NaCl being generated from the aerosol generator into another box specifically marked for scattering aerosols. For these tests, the solution concentrations of NaCl used to generate the aerosols were 0.15 g L^{-1} and 0.5 g L^{-1}. For these tests the only instruments used were the AE-52 and the OPS. This is due to the AE-51 being designed to collect aerosols with absorbing properties. The OPS results are only presented for the bins that sum to the concentration of $PM_{2.5}$, just like the black carbon experiments. Figure 3.16 shows the breakdown of particles that entered the OPS by size. All of the particles are smaller than approximately one micron due to the aerosol generator being designed to produce sub-micron aerosols. Figure 3.17 shows the results of the NaCl aerosol mass concentration from the OPS and the AE-52. After comparing the results of the OPS and the AE-52, it appears that the AE-52 is underestimating the amount of NaCl that is making it through the inlet tube and onto the filter strip inside the microAeth by a factor of ten, which is consistent with the 0.15 g L^{-1} BC results.

The same calculations were completed for the OPS during the 0.5 g L^{-1} NaCl box tests. Figure 3.18 shows the results from the OPS and AE-52 averaged from February through April 2014. After comparing the two instruments, it is apparent the AE-52 is again under estimating the concentration of aerosols by a factor of ten. The OPS was started at the same time as aerosol generation, but it took a few minutes for the aerosols to reach the inlet chamber of the OPS, which is why the shape of the graph in Figure 3.18 is gradually increasing. The AE-52 was also started at the exact time of the aerosol generator but because the inlet tubes are more streamlined and shorter than the OPS, the aerosol takes less time to impact the filter and increase attenuation.
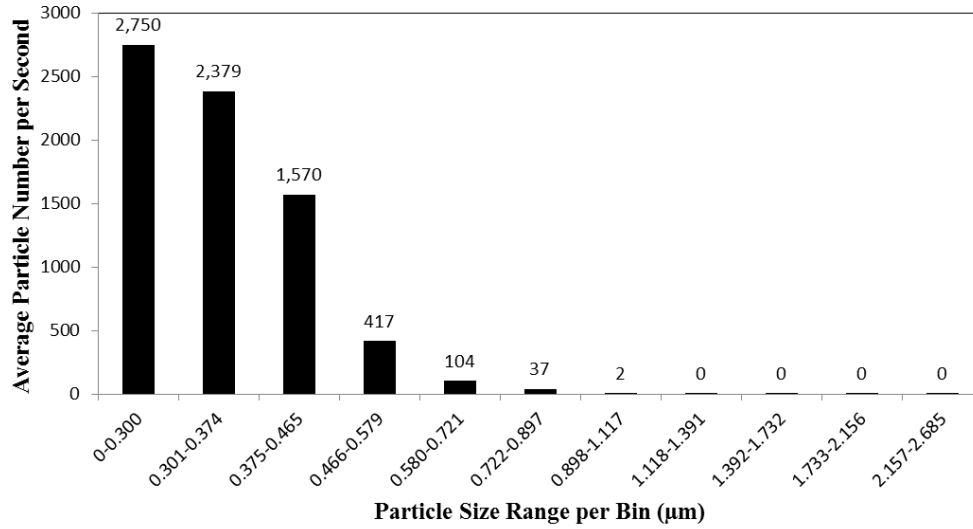
Figure 3.16. The breakdown of the number of particles per bin in the OPS during the NaCl box tests.
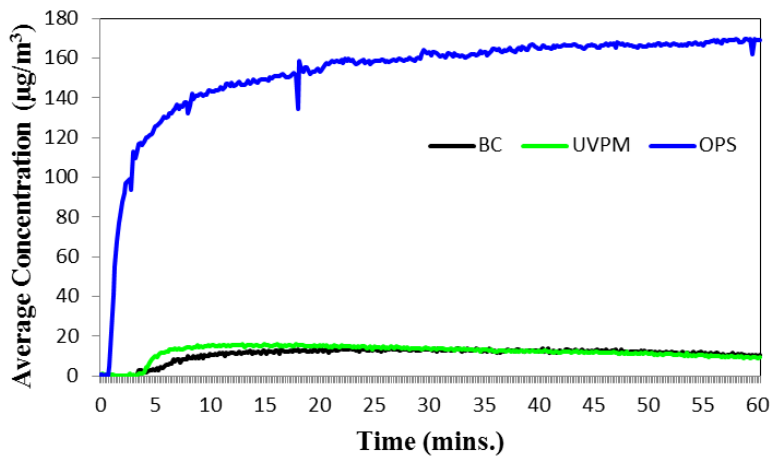

Figure 3.17. Results from the OPS and AE-52 during the 0.15 g L^{-1} NaCl box test.
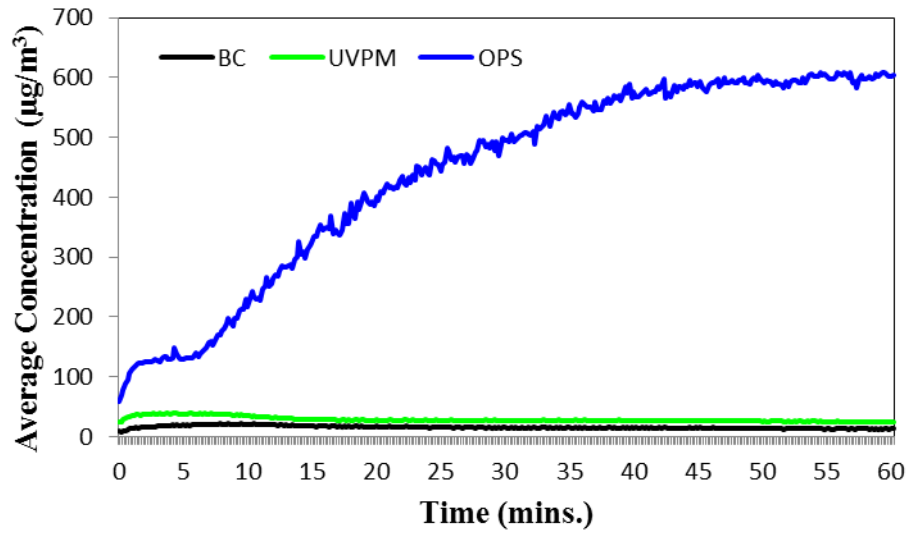
Figure 3.18. Data collected from the OPS and AE-52 during the 0.50 g L^{-1} NaCl box test.

The two microAethalometers were also used in small, hot fires in the fume hood of Dr. Cahill's laboratory (Figure 2.15). The fires only lasted approximately ten minutes each but they gave off enough smoke that the microAeths collected very high concentrations of $PM_{2.5}$, and the OPS collected very high concentrations of PM_1. Figure 3.19 shows the breakdown of aerosols into each bin of the OPS. The values are significantly higher during the second fire because it was easier to start the second fire and the smoke went more towards the inlets. Figure 3.20 shows the concentration of aerosols collected during the first fire. The microAeths read very consistently with each other, which was also the result from the BC box tests. Figure 3.21 shows the aerosol concentration collected during the second lab fire. The concentrations differ from the first fire because more paper was used to ignite the second fire than during the first fire which burned the same type of fuel (paper birch). Lastly, Figure 3.22 shows the OPS data collected during both fires. This is the first time that the microAeths consistently matched the OPS concentrations. A possible explanation for this is the fact that the microAeths were inside the fume hood only one foot in length away from the smoke. There was not enough room for the OPS to sit in the fume hood during the fires so it was positioned outside, on the lab bench, with an extended inlet tube reaching into the fume hood to collect the smoke aerosols. The reason for the decrease in concentration recorded by the OPS during the second fire could be due to different smoke dynamics. The fume hood door was opened during the second fire which could have allowed the smoke to dissipate into the lab and not enter the instrument.

Based on the data collected, the detection limits of the microAethalometers need to be adjusted. The quoted detection range for the microAeth was zero to one milligram per cubic meter and the small lab fires in the fume hood produced as high as 16.3 mg m^{-3}. The quoted

detection range also comes into question from the RxCADRE results where the AE-52 oversaturated at 600 µg m^{-3} (Figure 3.1).
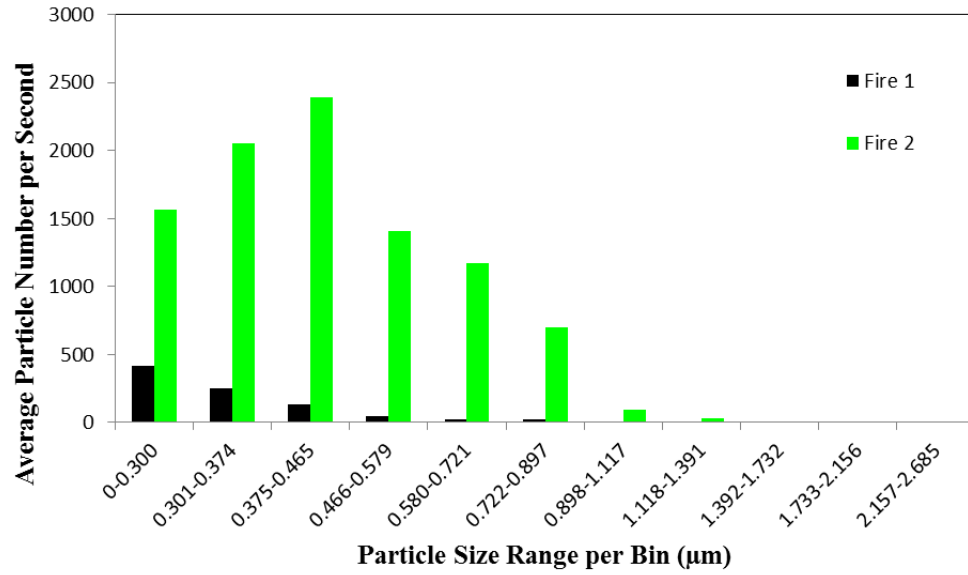
Figure 3.19. The amount of particles in each bin of the OPS during both fires in the laboratory fume hood.
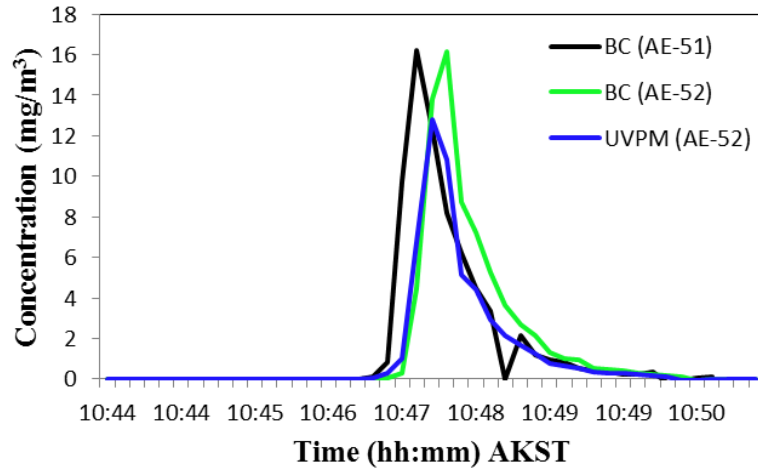
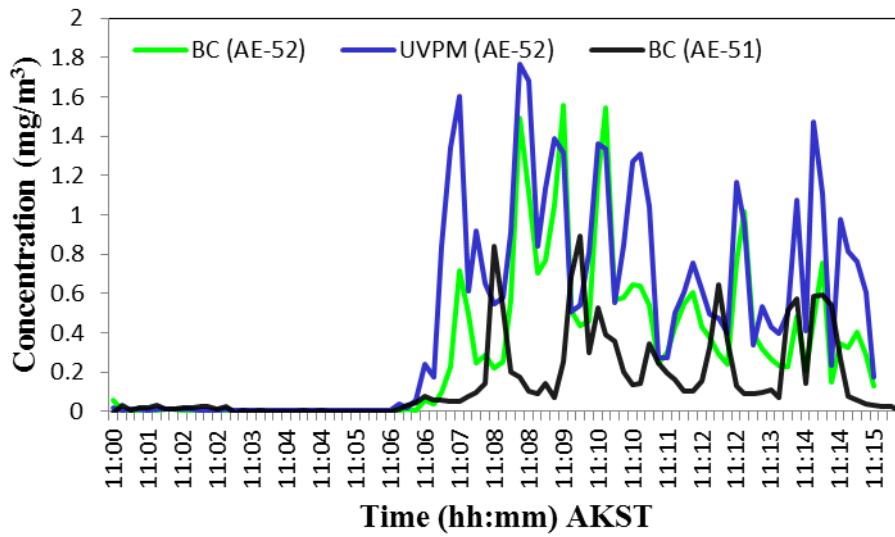Figure 3.20. Results from both the AE-51 and AE-52 during the first lab fire.

Figure 3.21. Results from both the AE-51 and AE-52 during the second lab fire.
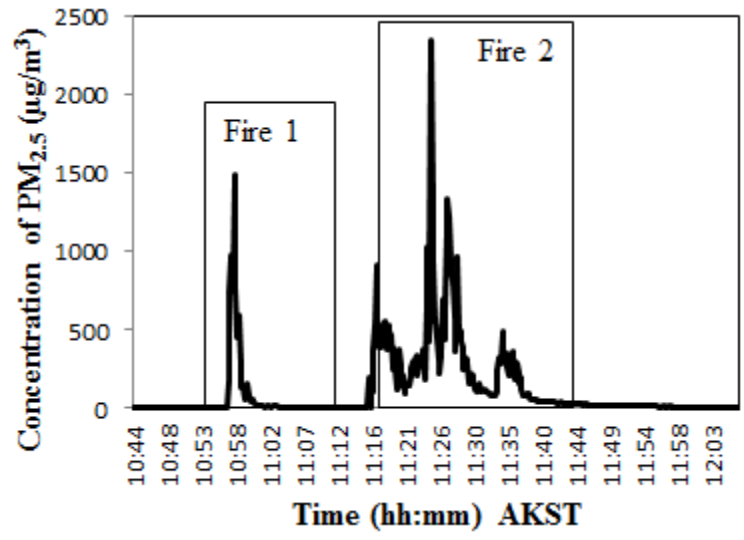
Figure 3.22. The OPS data collected during both lab fires.

Chapter 4 – Conclusion

The RxCADRE campaign, from October 31st to November 6th 2012 at Eglin Air Force Base, Florida provided an opportunity to study black carbon aerosols emitted from a prescribed fire smoke plume in real time. The RxCADRE scientific goals for researchers from the University of Alaska Fairbanks were to successfully integrate and fly a ground-based microAethalometer on a Boeing ScanEagle and collect black carbon aerosol concentrations in the smoke plume. During the campaign, four grass plots were burned. Ground-based sensors (microAethalometer and DustTrak DRX) collected smoke particulate data during the small-burn plots (S5-S3). After comparing the results collected from the ground based instruments, it was discovered there is an underestimation of the particulate concentration being recorded by the AE-52 microAethalometer and the DustTrak helped to confirm this point because there was a difference of approximately 1400 µg m^{-3} between the concentrations recorded by both instruments. This underestimation could be the result of particle shadowing, the fact that the microAeth measures the aerodynamic diameter of a particle and the DustTrak measures the geometric diameter of a particle, or the fact that the aethalometer only measures absorbing and organic particles and the DustTrak measures all particles. During the large plot burn, there was a successful integration and flight of the very first one-wavelength microAethalometer (AE-51) onto a Boeing ScanEagle by scientists at the University of Alaska Fairbanks. Having the BC sensor onboard the UAS allowed for real-time airborne aerosol measurements within the smoke plume. The integration was successful, and the instrument showed a large increase in BC aerosols when the plume was impacted by the ScanEagle at 10:04 AKST. The payload performance did not appear to be influenced in any way during flight, compared to operations on the ground.

The microAeths were also flown on the Polar Pumpkin, piloted by Art Mortvedt, to sample airborne BC between Fairbanks, Alaska and the geographic North Pole, and to observe how effective the microAeths were in high wind conditions as well as extreme cold temperatures. The microAeths experienced operational challenges in making BC measurements during the flight, but some aerosols were collected successfully. The study proved the microAeths are highly sensitive to high winds and an error message occurs if the flow rate is not set properly to counteract the ram air pressure. The polar flight also proved that the cold temperatures diminish the battery life of the instruments.

The AE-52 microAethalometer was also used to monitor the smoke from the Nenana Fire in the summer of 2013. The fire, which burned over 80 acres of white spruce, was approximately 30 miles south of Fairbanks, AK, but when the plume reached the instruments, significant concentrations of aerosols were recorded. After two hours of sampling the concentrations start to level out indicating thorough mixing of the boundary layer. The microAethalometer could be used as an everyday instrument to monitor BC concentrations, especially during fire season in Alaska and around the world.

The DustTrak was used from December 2012 to January 2013 during the Sled Dog Air Contaminant campaign. The study was done to determine the amount of $PM_{2.5}$ the sled dogs around the area were exposed to at their kennels. After the completion of the experiment it was discovered that the dogs were being exposed to concentrations over ten times the limit for the EPA ambient air quality standard. These findings can be attributed to the large concentration of emissions trapped near the earth's surface by an atmospheric inversion layer present over interior Alaska during the winter months.

Laboratory experiments were carried out to validate the results researchers obtained at RxCADRE. It was proven that the microAethalometer does in fact underestimate the amount of aerosol entering the inlet chamber. It was also proven that the AE-51 and AE-52 read BC aerosols at the same concentrations. Two optical particle sizers were used alongside the microAeths to verify the size of the aerosol that is entering the instrument as well as verify the concentrations the microAeth was recording. The OPSs helped confirm the underestimation of aerosol concentration by the microAeths.

4.1 Future Work

Airborne sampling of black carbon and other aerosols on small UASs is a new and emerging field. New instruments will provide aerosol researchers and atmospheric scientists with an improved understanding of the spatial and temporal distributions of aerosols in the atmosphere. There are multiple lines of development and experimentation arising from the work presented in this thesis that will help advance this field:

First, the integration of the microAethalometer on different unmanned aircraft is a major goal, so the sensor can become a standardly used instrument for UAS-based BC measurements around the world. Unmanned aircraft can be used in climate research to help map boundaries, observe changes in surface area, etc. by conducting regular flights over the same path. Currently, there is limited airborne data so being able to conduct a flight with multiple aircraft on the same track would be very beneficial. The multiple aircraft would provide the validation needed to allow UAS-based instruments to become more common in climate research. Also, the weight restrictions onboard a UAS is a current issue since the number of instruments onboard is

72

limited. The ScanEagle cannot currently sample for multiple instruments since the aircraft is strongly restricted by payload size and weight.

Second, laboratory work will help to troubleshoot the microAeth so there is a better understanding of why there is an underestimation of aerosol concentration. Further research must be done to determine if particle shadowing is the cause, or if the main issues are: 1) that the microAeth only measures aerodynamic diameter versus the DustTrak and OPS which only measure geometric diameter or 2) that the aethalometer only measures absorbing and organic particles and the DustTrak and OPS measure all particles. More sampling of aerosols needs to be done to determine the true detection limit of the instrument. Currently, the concentration range measurable by the microAeth, listed in the instrument operation manual, is 0-1 mg BC m^{-3}, but the true limits of the sensor need to be tested to determine how sensitive the microAeth is to various aerosol compositions and concentrations because this thesis proved the detection limit was wrong and the instrument is capable of higher concentrations. Also, in the laboratory, aerosols of different compositions should be generated using the aerosol generator and optical particle counter to help calibrate the microAeth for aerosols other than black carbon and sodium chloride. During a fire, the instrument could suck up dust, sulfates, metals, etc. so other analysis, to determine the true composition of the particulates, would be helpful. Other kinds of analysis could include using x-ray fluorescence or scanning electron microscopy. The microAeth filter strip could be analyzed in these instruments to get the true elemental composition of the sample.

Third, making the microAethalometers resistant to oversaturation, by installing a rolling filter strip, would greatly help the instrument become a true airborne instrument. Some engineering would need to take place to adapt the current model into an instrument that is just as compact but with the ability to move the filter strip away from an aerosol-saturated spot to a

73

clean spot on the substrate without having to bring the aircraft back to base to have a human physically change the strip. Pre-flight and post-flight calibration procedures need to be developed as well in order to assure quality data from future UAS deployments. Furthering these topics in the future would greatly help the microAeth become a universal and efficient instrument for the airborne sampling of aerosols in highly polluted areas such as Bangladesh and heavy industrial areas around the world.

References

1. Mayer, H., Air pollution in cities. *Atmospheric Environment* **1999,** *33*, (24–25), 4029-4037.

2. Fenger, J., Urban air quality. *Atmospheric Environment* **1999,** *33*, (29), 4877-4900.

3. Dockery, D. W.; Pope, C. A.; Xu, X.; Spengler, J. D.; Ware, J. H.; Fay, M. E.; Ferris, B. G.; Speizer, F. E., An Association between Air Pollution and Mortality in Six U.S. Cities. *New England Journal of Medicine* **1993,** *329*, (24), 1753-1759.

4. Baron, P. A.; Willeke, K., *Aerosol measurement: principles, techniques, and applications*. Second ed.; John Wiley & Sons: 2001.

5. Whitby, K.; Cantrell, B. In *Fine particles*, International Conference on Environmental Sensing and Assessment, Las Vegas, NV, Institute of Electrical and Electronic Engineers, 1976; 1976.

6. Kerminen, V.-M.; Virkkula, A.; Hillamo, R.; Wexler, A. S.; Kulmala, M., Secondary organics and atmospheric cloud condensation nuclei production. *Journal of Geophysical Research: Atmospheres* **2000,** *105*, (D7), 9255-9264.

7. Seinfeld, J. H.; Pandis, S. N., *Atmospheric chemistry and physics: from air pollution to climate change*. John Wiley & Sons: 2012.

8. Lamb, H., *Hydrodynamics*. **1995,** *Sixth Edition*.

9. Siegmann, K.; Scherrer, L.; Siegmann, H. C., Physical and chemical properties of airborne nanoscale particles and how to measure the impact on human health. *Journal of Molecular Structure: THEOCHEM* **1998,** *458*, (1–2), 191-201.

10.   Dockery, D. W.; Speizer, F. E.; Stram, D. O.; Ware, J. H.; Spengler, J. D.; Ferris, B. G., Effects of Inhalable Particles on Respiratory Health of Children. *American Review of Respiratory Disease* **1989,** *139*, (3), 587-594.

11.   Pope, I. C.; Burnett, R. T.; Thun, M. J.; et al., LUng cancer, cardiopulmonary mortality, and long-term exposure to fine particulate air pollution. *JAMA* **2002,** *287*, (9), 1132-1141.

12.   Schwartz, J.; Dockery, D. W.; Neas, L. M., Is Daily Mortality Associated Specifically with Fine Particles? *Journal of the Air & Waste Management Association* **1996,** *46*, (10), 927-939.

13.   Miller, T. P.; Casadevall, T. J., Volcanic ash hazards to aviation. *Encyclopedia of volcanoes* **2000**, 915-930.

14.   Rosenthal, J.; Battalino, T.; Eddington, L.; Helvey, R.; Fisk, C.; Lea, D., Aerosol Transport and Origins. *EO Propagation, Signature and System Performance Under Adverse Meteorological Conditions Considering Out-of-Area Operations* **1998**.

15.   Cahill, C. F., Asian aerosol transport to Alaska during ACE-Asia. *Journal of Geophysical Research: Atmospheres (1984–2012)* **2003,** *108*, (D23).

16.   Braaten, D. A.; Cahill, T. A., Size and composition of Asian dust transported to Hawaii. *Atmospheric Environment (1967)* **1986,** *20*, (6), 1105-1109.

17.   Li, J.; Wang, Z.; Zhuang, G.; Luo, G.; Sun, Y.; Wang, Q., Mixing of Asian mineral dust with anthropogenic pollutants over East Asia: a model case study of a super-duststorm in March 2010. *Atmos. Chem. Phys.* **2012,** *12*, (16), 7591-7607.

18.   Andreae, M. O.; Crutzen, P. J., Atmospheric Aerosols: Biogeochemical Sources and Role in Atmospheric Chemistry. *Science* **1997,** *276*, (5315), 1052-1058.

19.   Ramanathan, V.; Carmichael, G., Global and regional climate changes due to black carbon. *Nature Geosci* **2008,** *1*, (4), 221-227.

20.   Goldberg, E. D., Black carbon in the environment: properties and distribution. *Environmental science and technology (USA)* **1985**.

21.   Forster, P.; Ramaswamy, V.; Artaxo, P.; Berntsen, T.; Betts, R.; Fahey, D. W.; Haywood, J.; Lean, J.; Lowe, D. C.; Myhre, G., Changes in atmospheric constituents and in radiative forcing. Chapter 2. In *Climate Change 2007. The Physical Science Basis*, 2007.

22.   Viidanoja, J.; Sillanpää, M.; Laakia, J.; Kerminen, V.-M.; Hillamo, R.; Aarnio, P.; Koskentalo, T., Organic and black carbon in $PM_{2.5}$ and PM_{10}: 1 year of data from an urban site in Helsinki, Finland. *Atmospheric Environment* **2002,** *36*, (19), 3183-3193.

23.   Rodhe, H.; Persson, C.; Åkesson, O., An investigation into regional transport of soot and sulfate aerosols. *Atmospheric Environment (1967)* **1972,** *6*, (9), 675-693.

24.   Wang, Y.; Hopke, P. K.; Rattigan, O. V.; Zhu, Y., Characterization of ambient black carbon and wood burning particles in two urban areas. *Journal of Environmental Monitoring* **2011,** *13*, (7), 1919-1926.

25.   Penner, J. E.; Novakov, T., Carbonaceous particles in the atmosphere: A historical perspective to the Fifth International Conference on Carbonaceous Particles in the Atmosphere. *Journal of Geophysical Research: Atmospheres* **1996,** *101*, (D14), 19373-19378.

26.   Flanner, M. G.; Zender, C. S.; Randerson, J. T.; Rasch, P. J., Present-day climate forcing and response from black carbon in snow. *Journal of Geophysical Research: Atmospheres* **2007,** *112*, (D11), D11202.

27. Ozartan, M.; Akgul, S.; Akca, B. In *A different view to future use of unmanned aerial vehicles*, Unmanned Aircraft Systems (ICUAS), 2013 International Conference on, 2013; IEEE: 2013; pp 167-172.

28. McGonigle, A.; Aiuppa, A.; Giudice, G.; Tamburello, G.; Hodson, A.; Gurrieri, S., Unmanned aerial vehicle measurements of volcanic carbon dioxide fluxes. *Geophysical Research Letters* **2008,** *35*, (6).

29. Ramana, M.; Ramanathan, V.; Kim, D.; Roberts, G.; Corrigan, C., Albedo, atmospheric solar absorption and heating rate measurements with stacked UAVs. *Quarterly Journal of the Royal Meteorological Society* **2007,** *133*, (629), 1913-1931.

30. Roberts, G. C.; Ramana, M. V.; Corrigan, C.; Kim, D.; Ramanathan, V., Simultaneous observations of aerosol–cloud–albedo interactions with three stacked unmanned aerial vehicles. *Proceedings of the National Academy of Sciences* **2008,** *105*, (21), 7370-7375.

31. Corrigan, C.; Roberts, G.; Ramana, M.; Kim, D.; Ramanathan, V., Capturing vertical profiles of aerosols and black carbon over the Indian Ocean using autonomous unmanned aerial vehicles. *Atmospheric Chemistry and Physics* **2008,** *8*, (3), 737-747.

32. Everaerts, J., The use of unmanned aerial vehicles (UAVs) for remote sensing and mapping. *The International Archives of the Photogrammetry, Remote Sensing and Spatial Information Sciences* **2008,** *37*, 1187-1192.

33. Borchardt, J. K., Unmanned aerial vehicles spur composites use. *Reinforced Plastics* **2004,** *48*, (4), 28-31.

34. Ferrero, L.; Mocnik, G.; Ferrini, B. S.; Perrone, M. G.; Sangiorgi, G.; Bolzacchini, E., Vertical profiles of aerosol absorption coefficient from micro-Aethalometer data and Mie calculation over Milan. *Science of The Total Environment* **2011,** *409*, (14), 2824-2837.

35.   Hansen, A.; Mocnik, G. In *The``Micro''Aethalometer-an enabling technology for new applications in the measurement of Aerosol Black Carbon*, AGU Fall Meeting Abstracts, 2010; 2010; p 0194.

36.   Weingartner, E.; Saathoff, H.; Schnaiter, M.; Streit, N.; Bitnar, B.; Baltensperger, U., *Absorption of light by soot particles: determination of the absorption coefficient by means of aethalometers*. *Aerosol Science* **2003,** 34, 1445-1463.

37.   Jeong, C.-H.; Hopke, P. K.; Kim, E.; Lee, D.-W., The comparison between thermal-optical transmittance elemental carbon and Aethalometer black carbon measured at multiple monitoring sites. *Atmospheric Environment* **2004,** *38*, (31), 5193-5204.

38.   Park, K.; Chow, J. C.; Watson, J. G.; Trimble, D. L.; Doraiswamy, P.; Park, K.; Arnott, W. P.; Stroud, K. R.; Bowers, K.; Bode, R., Comparison of continuous and filter-based carbon measurements at the Fresno Supersite. *Journal of the Air & Waste Management Association* **2006,** *56*, (4), 474-491.

39.   Sandradewi, J.; Prévôt, A.; Weingartner, E.; Schmidhauser, R.; Gysel, M.; Baltensperger, U., A study of wood burning and traffic aerosols in an Alpine valley using a multi-wavelength Aethalometer. *Atmospheric Environment* **2008,** *42*, (1), 101-112.